White Dwarf Rotation as a Function of Mass and a Dichotomy of Mode Line Widths: *Kepler* Observations of 27 Pulsating DA White Dwarfs through *K2* Campaign 8

J. J. Hermes[1,6], B. T. Gänsicke[2], Steven D. Kawaler[3], S. Greiss[2], P.-E. Tremblay[2], N. P. Gentile Fusillo[2], R. Raddi[2],
S. M. Fanale[1], Keaton J. Bell[4], E. Dennihy[1], J. T. Fuchs[1], B. H. Dunlap[1], J. C. Clemens[1], M. H. Montgomery[4],
D. E. Winget[4], P. Chote[2], T. R. Marsh[2], and S. Redfield[5]

[1] Department of Physics and Astronomy, University of North Carolina, Chapel Hill, NC 27599, USA; jjhermes@unc.edu
[2] Department of Physics, University of Warwick, Coventry CV4 7AL, UK
[3] Department of Physics and Astronomy, Iowa State University, Ames, IA 50011, USA
[4] Department of Astronomy, University of Texas at Austin, Austin, TX 78712, USA
[5] Wesleyan University Astronomy Department, Van Vleck Observatory, 96 Foss Hill Drive, Middletown, CT 06459, USA

Abstract

We present photometry and spectroscopy for 27 pulsating hydrogen-atmosphere white dwarfs (DAVs; a.k.a. ZZ Ceti stars) observed by the *Kepler* space telescope up to *K2* Campaign 8, an extensive compilation of observations with unprecedented duration (>75 days) and duty cycle (>90%). The space-based photometry reveals pulsation properties previously inaccessible to ground-based observations. We observe a sharp dichotomy in oscillation mode line widths at roughly 800 s, such that white dwarf pulsations with periods exceeding 800 s have substantially broader mode line widths, more reminiscent of a damped harmonic oscillator than a heat-driven pulsator. Extended *Kepler* coverage also permits extensive mode identification: we identify the spherical degree of 87 out of 201 unique radial orders, providing direct constraints of the rotation period for 20 of these 27 DAVs, more than doubling the number of white dwarfs with rotation periods determined via asteroseismology. We also obtain spectroscopy from 4 m-class telescopes for all DAVs with *Kepler* photometry. Using these homogeneously analyzed spectra, we estimate the overall mass of all 27 DAVs, which allows us to measure white dwarf rotation as a function of mass, constraining the endpoints of angular momentum in low- and intermediate-mass stars. We find that 0.51–$0.73\,M_\odot$ white dwarfs, which evolved from 1.7–$3.0\,M_\odot$ ZAMS progenitors, have a mean rotation period of 35 hr with a standard deviation of 28 hr, with notable exceptions for higher-mass white dwarfs. Finally, we announce an online repository for our *Kepler* data and follow-up spectroscopy, which we collect at http://k2wd.org.

Key words: stars: oscillations – stars: variables: general – white dwarfs

Supporting material: machine-readable tables

1. Introduction

Isolated white dwarf stars have been known for more than half a century to vary in brightness on short timescales (Landolt 1968). The roughly 2–20 minute flux variations are known to result from surface temperature changes caused by non-radial *g*-mode pulsations excited by surface convection (see reviews by Fontaine & Brassard 2008; Winget & Kepler 2008; Althaus et al. 2010).

Given the potential of asteroseismology to discern their interior structure, white dwarfs have been the targets of extensive observing campaigns to accurately measure their periods, which can then be compared to theoretical models to probe deep below the surface of these stellar remnants. Early observations of white dwarfs showed pulsations at many periods within the same star, further demonstrating their asteroseismic potential (Warner & Robinson 1972). However, observations from single sites were complicated by aliases arising from gaps in data collection.

Starting in the late 1980s, astronomers combated day–night aliasing by establishing the Whole Earth Telescope, a cooperative optical observing network distributed in longitude around the Earth acting as a single instrument (Nather et al. 1990). Dozens of astronomers trekked to remote observatories across the globe for these labor-intensive campaigns, facing complications ranging from active hurricane seasons (O'Brien et al. 1998) to near-fatal stabbings (Vauclair et al. 2002). Many campaigns lasted up to several weeks with duty cycles better than 70%, delivering some of the most complete pictures of stellar structure and rotation in the 20th century for stars other than our Sun (e.g., Winget et al. 1991, 1994).

Given the resources required, however, only a few dozen pulsating white dwarfs have been studied with the Whole Earth Telescope. Pulsating hydrogen-atmosphere white dwarfs (DAVs; a.k.a. ZZ Ceti stars) are the most numerous pulsating stars in the Galaxy, but fewer than 10 were observed with this unified network.

The advent of space-based photometry from *CoRoT* and *Kepler* revolutionized the study of stellar interiors, ranging from *p*-modes in solar-like oscillators on the main sequence and red-giant branch (e.g., Chaplin & Miglio 2013) to *g*-modes in massive stars and hot subdwarfs (e.g., Degroote et al. 2010; Reed et al. 2011). For example, from *Kepler* we now have excellent constraints on core and envelope rotation in a wide range of stars (Aerts 2015). We have also seen new types of stochastic-like pulsations in classical heat-driven pulsators, such as δ Scuti stars (Antoci et al. 2011) and hot subdwarfs (Østensen et al. 2014).

However, this revolution did not immediately translate to white dwarf stars, few of which were identified or observed in

---
[6] Hubble Fellow.

Table 1
Target Selection Criterion for the First 27 Pulsating DA White Dwarfs Observed by *Kepler* and *K2*

KIC/EPIC	R.A. and Decl. (J2000.0)	Alt. Name	g (mag)	($u–g$,$g–r$) (AB mag)	($B–R$,$R–I$) (AB mag)	Source Catalog	*K2* Field	Proposal (GO)	Selection Method	Disc.
4357037	19 17 19.197+39 27 19.10	⋯	18.2	(0.50, −0.17)	⋯	KIS	K1	40109	Colors	1
4552982	19 16 43.827+39 38 49.69	⋯	17.7	⋯	(0.02, 0.03)	SSS	K1	40050	Colors	2
7594781	19 08 35.880+43 16 42.36	⋯	18.1	(0.56, −0.16)	⋯	KIS	K1	40109	Colors	1
10132702	19 13 40.893+47 09 31.28	⋯	19.0	(0.50, −0.16)	⋯	KIS	K1	40105	Colors	1
11911480	19 20 24.897+50 17 21.32	⋯	18.0	(0.43, −0.16)	⋯	KIS	K1	40105	Colors	3
60017836	23 38 50.740−07 41 19.90	GD 1212	13.3	⋯	⋯	⋯	Eng	DDT	KnownZZ	4
201355934	11 36 04.013−01 36 58.09	WD 1133−013	17.8	(0.46, −0.17)	⋯	SDSS	C1	1016	KnownZZ	5
201719578	11 22 21.104+03 58 22.41	WD 1119+042	18.1	(0.39, −0.01)	⋯	SDSS	C1	1016	KnownZZ	6
201730811	11 36 55.157+04 09 52.80	WD 1134+044	17.1	(0.49, −0.11)	⋯	SDSS	C1	1015	Spec. T_{eff}	7
201802933	11 51 26.147+05 25 12.90	⋯	17.6	(0.42, −0.19)	⋯	SDSS	C1	1016	Colors	⋯
201806008	11 51 54.200+05 28 39.82	PG 1149+058	14.9	(0.45, −0.13)	⋯	SDSS	C1	1016	KnownZZ	8
206212611	22 20 24.230−09 33 31.09	⋯	17.3	(0.47, −0.14)	⋯	SDSS	C3	3082	Colors	⋯
210397465	03 58 24.233+13 24 30.79	⋯	17.6	(0.65, −0.12)	⋯	SDSS	C4	4043	Colors	⋯
211596649	08 32 03.984+14 29 42.37	⋯	18.9	(0.54, −0.18)	⋯	SDSS	C5	5073	Colors	⋯
211629697	08 40 54.142+14 57 08.98	⋯	18.3	(0.46, −0.15)	⋯	SDSS	C5	5043	Spec. T_{eff}	⋯
211914185	08 37 02.160+18 56 13.38	⋯	18.8	(0.36, −0.21)	⋯	SDSS	C5	5073	Colors	9
211916160	08 56 48.334+18 58 04.92	⋯	18.9	(0.40, −0.13)	⋯	SDSS	C5	5073	Colors	⋯
211926430	09 00 41.080+19 07 14.40	⋯	17.6	(0.47, −0.20)	⋯	SDSS	C5	5017	Spec. T_{eff}	⋯
228682478	08 40 27.839+13 20 09.96	⋯	18.2	(0.35, −0.14)	⋯	SDSS	C5	5043	Colors	⋯
229227292	13 42 11.621−07 35 40.10	⋯	16.6	(0.46, −0.12)	⋯	ATLAS	C6	6083	Colors	⋯
229228364	19 18 10.598−26 21 05.00	⋯	17.8	⋯	(0.10, 0.03)	SSS	C7	7083	Colors	⋯
220204626	01 11 23.888+00 09 35.15	WD 0108−001	18.4	⋯	⋯	SDSS	C8	8018	Spec. T_{eff}	7
220258806	01 06 37.032+01 45 03.01	⋯	16.2	(0.41, −0.21)	⋯	SDSS	C8	8018	Colors	⋯
220347759	00 51 24.245+03 39 03.79	PHL 862	17.6	(0.43, −0.18)	⋯	SDSS	C8	8018	Colors	⋯
220453225	00 45 33.151+05 44 46.96	⋯	17.9	(0.42, −0.15)	⋯	SDSS	C8	8018	Colors	⋯
229228478	01 22 34.683+00 30 25.81	GD 842	16.9	(0.43, −0.19)	⋯	SDSS	C8	8018	KnownZZ	5
229228480	01 11 00.638+00 18 07.15	WD 0108+000	18.8	(0.45, −0.17)	⋯	SDSS	C8	8018	KnownZZ	6

References. Discovery of pulsations announced by (1) Greiss et al. (2016); (2) Hermes et al. (2011); (3) Greiss et al. (2014); (4) Giannias et al. (2006); (5) Castanheira et al. (2010); (6) Mukadam et al. (2004); (7) Pyrzas et al. (2015)—search for DAVs in WD+dM systems; (8) Voss et al. (2006); (9) Hermes et al. (2017c).

(This table is available in machine-readable form.)

the original *Kepler* mission. We aim to rectify that shortfall with an extensive search for pulsating white dwarfs observable by *K2*. After the failure of its second reaction wheel, *Kepler* entered a new phase of observations, *K2*, where it observes new fields along the ecliptic every three months (Howell et al. 2014). This has significantly expanded the number of white dwarfs available for extended observations. We targeted all suitable candidate pulsating white dwarfs to provide a legacy of high-cadence, extended light curves.

We present here an omnibus analysis of the first 27 DAVs observed by the *Kepler* space telescope, including follow-up spectroscopy to measure their atmospheric parameters. Only six of the DAVs presented here were known to pulsate prior to their *Kepler* observations, and only two of those six had more than 3 hr of previous time-series photometry.

Our manuscript is organized as follows. In Section 2, we outline our target selection, and we describe our space-based photometry in Section 3. We detail our spectroscopic observations from the 4.1 m SOAR telescope and present our full sample analysis in Section 4. The first part of our light curve analysis, in Section 5, centers on mode stability as a function of pulsation period. We summarize some of the large-scale trends we see in the DAV instability strip as observed by *Kepler* and *K2* in Section 6. We then explore the asteroseismic rotation periods of 20 of the 27 DAVs in our sample, and place the first constraints on white dwarf rotation as a function of

mass in Section 7. We conclude with notes on individual objects in Section 8, as well as final discussions and conclusions in Section 9. Table 5 in the Appendix features all pulsations discovered and analyzed here: 389 entries corresponding to 201 independent modes of unique radial order (k) and spherical degree (ℓ) in 27 different stars, the most extensive new listing of white dwarf pulsations ever compiled.

2. Candidate DAV Target Selection

Table 1 details the selection criteria for the first 27 DAVs observed by *Kepler* with short-cadence (∼1 minute) exposures through *K2* Campaign 8 and analyzed here, including the Guest Observer (GO) program under which the target was proposed for short-cadence observations.

White dwarfs hotter than 10,000 K are most effectively selected based on their blue colors and relatively high proper motions (e.g., Gentile Fusillo et al. 2015). However, only two white dwarfs were known in the 105 square-degree *Kepler* field two years prior to its launch in 2009: WD 1942+499 and WD 1917+461. An extensive search in the year before launch —mostly from *Galex* ultraviolet excess sources and faint blue objects with high proper motions—uncovered just a dozen additional white dwarfs in the original *Kepler* field (Østensen et al. 2010), with just one pulsating (Østensen et al. 2011).

Table 2
Details of Short-cadence Photometry of the First 27 Pulsating DA White Dwarfs Observed by *Kepler* and *K2*

KIC/EPIC	K2 Field	K_p (mag)	Data Rel.	CCD Chan.	Ap. (px)	Targ. Frac.	T_0 (BJD$_{TDB}$ −2454833.0)	Dur. (days)	Duty (%)	Res. (μHz)	1% FAP (ppt)	0.1% FAP (ppt)	$5\langle A\rangle$ (ppt)	WMP (s)	Pub.
4357037	K1	18.0	25	68	1	0.55	1488.657916	36.31	98.9	0.159	1.018	1.050	0.963	358.1	⋯
4552982	K1	17.9	25	68	4	0.85	1099.398257	82.63	88.1	0.070	0.722	0.722	0.665	778.2	1
7594781	K1	18.2	25	45	1	0.52	1526.113126	31.84	99.3	0.182	0.749	0.781	0.664	333.3	⋯
10132702	K1	18.8	25	48	2	0.61	1373.478019	97.67	91.8	0.059	1.431	1.483	1.441	749.3	⋯
11911480	K1	17.6	25	2	2	0.48	1472.087602	85.86	84.7	0.067	0.764	0.794	0.766	276.9	2
60017836	Eng.	13.3	−1	76	93	0.97	1860.040459	8.91	98.9	0.649	0.284	0.297	0.172	1019.1	3
201355934	C1	17.9	14	39	4	0.33	1975.168594	77.52	92.9	0.075	0.478	0.493	0.462	208.2	⋯
201719578	C1	18.1	14	67	11	0.88	1975.168222	78.80	94.7	0.073	0.956	0.993	0.883	740.9	⋯
201730811	C1	17.1	14	46	8	0.98	1975.168490	77.18	94.7	0.075	0.253	0.262	0.242	248.4	4
201802933	C1	17.7	14	29	11	0.95	1975.168648	77.24	94.9	0.075	0.605	0.630	0.592	266.2	⋯
201806008	C1	15.0	14	29	33	0.91	1975.168653	78.91	95.3	0.073	0.311	0.322	0.162	1030.4	⋯
206212611	C3	17.4	10	46	6	0.97	2144.093232	69.18	98.3	0.084	0.304	0.314	0.321	1204.4	⋯
210397465	C4	17.7	10	54	8	0.96	2228.790357	70.90	98.7	0.082	0.945	0.980	0.879	841.0	⋯
211596649	C5	19.0	10	58	4	0.99	2306.600768	74.84	98.7	0.077	1.695	1.762	1.809	288.7	⋯
211629697	C5	18.4	10	38	5	0.98	2306.600916	74.84	98.7	0.077	0.758	0.784	0.772	1045.2	⋯
211914185	C5	18.9	10	46	5	0.97	2306.600805	74.84	98.7	0.077	0.922	0.955	0.976	161.7	5
211916160	C5	19.0	10	25	6	0.82	2306.601137	74.84	98.5	0.077	1.191	1.237	1.256	201.3	⋯
211926430	C5	17.7	10	9	6	0.96	2306.601189	74.84	98.4	0.077	0.471	0.486	0.456	244.2	⋯
228682478	C5	18.3	10	39	10	0.74	2306.600932	74.84	98.2	0.077	0.395	0.410	0.413	301.1	⋯
229227292	C6	16.7	8	48	4	0.98	2384.453493	78.93	98.2	0.073	0.347	0.357	0.277	964.5	⋯
229228364	C7	17.9	9	39	7	0.98	2467.250743	78.72	98.0	0.074	0.487	0.508	0.495	1116.4	⋯
220204626	C8	17.2	11	54	19	0.83	2559.058649	78.72	98.3	0.074	0.805	0.832	0.846	642.7	⋯
220258806	C8	16.4	11	59	8	0.90	2559.058611	78.72	96.0	0.074	0.155	0.161	0.154	206.0	⋯
220347759	C8	17.7	11	64	8	0.83	2559.058460	78.72	96.5	0.074	0.458	0.470	0.476	209.3	⋯
220453225	C8	18.0	11	68	9	0.93	2559.058403	78.72	96.7	0.074	0.625	0.646	0.631	1034.9	⋯
229228478	C8	17.0	11	35	22	0.97	2559.058796	78.72	98.5	0.074	0.514	0.534	0.535	141.8	⋯
229228480	C8	18.9	11	54	8	0.89	2559.058649	78.72	98.6	0.074	2.501	2.586	2.618	280.0	⋯

References. *Kepler*/*K2* data analyzed by (1) Bell et al. (2015); (2) Greiss et al. (2014); (3) Hermes et al. (2014); (4) Hermes et al. (2015a); (5) Hermes et al. (2017c).
(This table is available in machine-readable form.)

The most substantial deficiency for white dwarf selection came from the lack of existing blue photometry of the *Kepler* field, in either SDSS-u' or Johnson-U; in 2009, there was very little coverage from the Sloan Digital Sky Survey (SDSS) of the *Kepler* field. Two surveys filled this gap several years after *Kepler* launched: the *Kepler*-INT Survey (KIS), providing U–g–r–i–Hα photometry of the entire *Kepler* field (Greiss et al. 2012), and a U–V–B survey from Kitt Peak National Observatory (Everett et al. 2012).

The KIS proved to be an excellent resource for finding new pulsating white dwarfs; we used it to discover 10 new DAVs in the *Kepler* field (Greiss et al. 2016). Unfortunately, only five were observed before the failure of the spacecraft's second reaction wheel. *K2* has now afforded us the opportunity to observe dozens of new candidate pulsating white dwarfs in each new campaign pointing along the ecliptic.

DAV pulsations, excited by a hydrogen partial-ionization zone, occur in a narrow temperature range between roughly 12,600–10,600 K for canonical-mass ($0.6\,M_\odot$) white dwarfs (Tremblay et al. 2015). Therefore, the most efficient way to select candidate DAVs is to look for those with effective temperatures within the DAV instability strip. Empirically, this is best accomplished from Balmer-line fits to low-resolution spectroscopy, which is available for many white dwarfs in SDSS (e.g., Mukadam et al. 2004).

We targeted four new DAVs observed through *K2* Campaign 8 based on serendipitous SDSS spectroscopy, which revealed atmospheric parameters within the empirical instability strip (Kleinman et al. 2013). The majority of our new DAV candidates did not have spectroscopy and were selected based on their (u−g, g−r) colors, mostly from SDSS (Gentile Fusillo et al. 2015), plus one from (u−g, g−r) colors from an early data release of the VST ATLAS survey (Gentile Fusillo et al. 2017). Three color-selected white dwarfs in Campaign 5 were proposed for short-cadence *K2* observations for possible planetary transits (GO program 5073).

We also selected two DAVs from the Supercosmos Sky Survey (SSS) catalog of Rowell & Hambly (2011), identified as white dwarfs based on their proper motions and selected as DAV candidates through their (B−R, R−I) colors. This includes the white dwarf with the longest space-based light curve, observed in the original *Kepler* field (Hermes et al. 2011).

Finally, six DAVs observed by *K2* were known to pulsate before the launch of the spacecraft (KnownZZ). Our full selection information is summarized in Table 1, including the publication announcing the discovery of variability when relevant. We plan to publish our full list of candidate DAVs, including limits on those not observed to vary with *K2* observations, at the end of the mission.

We note that in fact, 29 DAVs were observed by the *Kepler* spacecraft through Campaign 8. However, we exclude two DAVs from our analysis here because they each have more than 100 significant periodicities deserving of their own individual analyses. Neither star appears to be in tension with our general trends or results. The excluded DAVs (EPIC 211494257 and

EPIC 212395381) will be detailed in two forthcoming publications.

3. Space-based *Kepler* Photometry

All observations analyzed here were collected by the *Kepler* spacecraft with short-cadence exposures, which are co-adds of the 9×6.02 s exposures for a total exposure time of 58.85 s, including readout overheads (Gilliland et al. 2010). Full details of the raw and processed *Kepler* and *K2* observations are summarized in Table 2.

For the five DAVs observed in the original *Kepler* mission, we analyzed the light curves processed by the GO office (Smith et al. 2012; Stumpe et al. 2012). We produced the final light curves using the calculated PDCSAP flux and flux uncertainties after iteratively clipping all points 5σ from the light curve median and fitting out a second-order polynomial to correct for any long-term instrumental drift. Only two DAVs in the original mission were observed for more than one quarter, and their full light curves have been analyzed elsewhere (Bell et al. 2015 for KIC 4552982 and Greiss et al. 2014 for KIC 11911480). Here we analyze only Q12 for KIC 4552982 and Q16 for KIC 11911480 to remain relatively consistent with the duration of the other DAVs observed with *K2*. All original-mission observations were extracted from data release 25, which includes updated smear corrections for short-cadence data[7], which is the cause of the amplitude discrepancy in KIC 11911480 observed by Greiss et al. (2014).

Reducing data obtained during the two-reaction-wheel-controlled *K2* mission requires more finesse, since the space-craft checks its roll orientation roughly every six hours and, if necessary, fires its thrusters to remain accurately pointed. Thruster firings introduce discontinuities into the photometry.

For each DAV observed with *K2*, we downloaded its short-cadence Target Pixel File from the Mikulski Archive for Space Telescopes and processed it using the PYKE software package managed by the *Kepler* GO office (Still & Barclay 2012). We began by choosing a fixed aperture that maximized the signal-to-noise ratio (S/N) of our target, extracted the target flux, and subsequently fit out a second-order polynomial to three-day segments to flatten longer-term instrumental trends. We subsequently used the KEPSFF task by Vanderburg & Johnson (2014) to mitigate the *K2* motion-correlated systematics. Finally, we iteratively clipped all points 5σ from the light curve median and fit out a second-order polynomial to the whole data set to produce a final light curve.[8]

We list the size of the final fixed aperture (Ap.) used for our extractions in Table 2, along with the CCD channel from which the observations were read out. Channel 48 and especially Channel 58 are susceptible to rolling band pattern noise, which can lead to long-term systematics in the light curve (see Section 3 of Hermes et al. 2017a and references therein).

We note the "Targ. Frac." column of Table 2, which estimates (on a scale from 0.0 to 1.0) the total fraction of the flux contained in the aperture that belongs to the target. This is important for crowded fields, since each *Kepler* pixel covers 4″ on a side. Amplitudes were not adjusted by this factor, which should be applied when comparing the pulsation amplitudes reported here to ground-based amplitudes or star-to-star

amplitude differences. Our target fraction values for DAVs in the original mission come from the *Kepler* Input Catalog (Brown et al. 2011). *K2* targets do not have such estimates, so we calculated the target fraction for DAVs in *K2* by modeling the point-spread function of our target and comparing the modeled flux of the target to the total flux observed in the extracted aperture. We perform this calculation using the pixel-response function tool KEPPRF in PYKE.

The light curves described here are the longest systematic look ever undertaken of white dwarf pulsations. All but three of the 27 DAVs have more than 69 days of observations with high duty cycles, in most cases exceeding 98%. This long-baseline coverage provides frequency resolution to better than 0.08 μHz in almost all cases. The high duty cycle ensures an exceptionally clean spectral window, easing the interpretation of the frequency spectra and simplifying mode identification.

Figure 1 highlights a representative amplitude spectrum for a hot DAV: EPIC 201802933 (SDSS J1151+0525, $K_p = 17.7$ mag), observed for more than 77 days in *K2* Campaign 1. All Fourier transforms we compute were oversampled by a factor of 20, calculated from the software package PERIOD04 (Lenz & Breger 2005). We fit for and removed all instrumental artifacts arising from the long-cadence sampling rate, at integer multiples of roughly 566.48 μHz (Gilliland et al. 2010). All panels of Figure 1 are on the same frequency scale, including the spectral window.

We computed a significance threshold for all DAVs from a shuffled simulation of the data, as described in Hermes et al. (2015a). In summary, we keep the time sampling of our observed light curves but randomly shuffle the flux values to create 10,000 synthetic light curves, noting the highest peak in the Fourier transform for each synthetic data set. We set our 1% (0.1%) False Alarm Probability (FAP) at the value for which 99% (99.9%) of these synthetic Fourier transforms do not have a peak exceeding that amplitude. We also list in Table 2 the value for five times the average amplitude of the entire Fourier transform, $5\langle A\rangle$.

For all DAVs, we adopt the 1% FAP as our significance threshold and produce a period list of observed pulsations, detailed in Table 5 in the Appendix. Our first set of uncertainties on the period, frequency, amplitude, and phase in Table 5 arise from a simultaneous nonlinear least-squares fit to the significant peaks, calculated with PERIOD04. All light curves are barycentric corrected, and the phases in Table 5 are relative to the first mid-exposure time (T_0) listed in Table 2. The frequencies of variability are not in the stellar rest frame, but many have high enough precision that they should eventually be corrected for the Doppler and gravitational redshift of the white dwarf (e.g., Davies et al. 2014).

Importantly, we are able to identify the spherical degree (ℓ) of 87 out of 201 independent modes in these DAVs (more than 40%), based on common frequency patterns in the Fourier transforms, which in turn illuminates the rotation periods of these stellar remnants (see Section 7). When identified, we group in Table 5 each set of frequencies of the same radial order (k) and spherical degree (ℓ), and include the measured frequency splittings. We relax the significance threshold for a handful of modes that share common frequency splittings, which occasionally helps with identifying the correct azimuthal order (m) for the modes present. We have not attempted to quantify the exact radial orders of any of the pulsations here, but leave that to future asteroseismic analysis of these stars.

---

[7] https://keplerscience.arc.nasa.gov/data/documentation/KSCI-19080-002.pdf

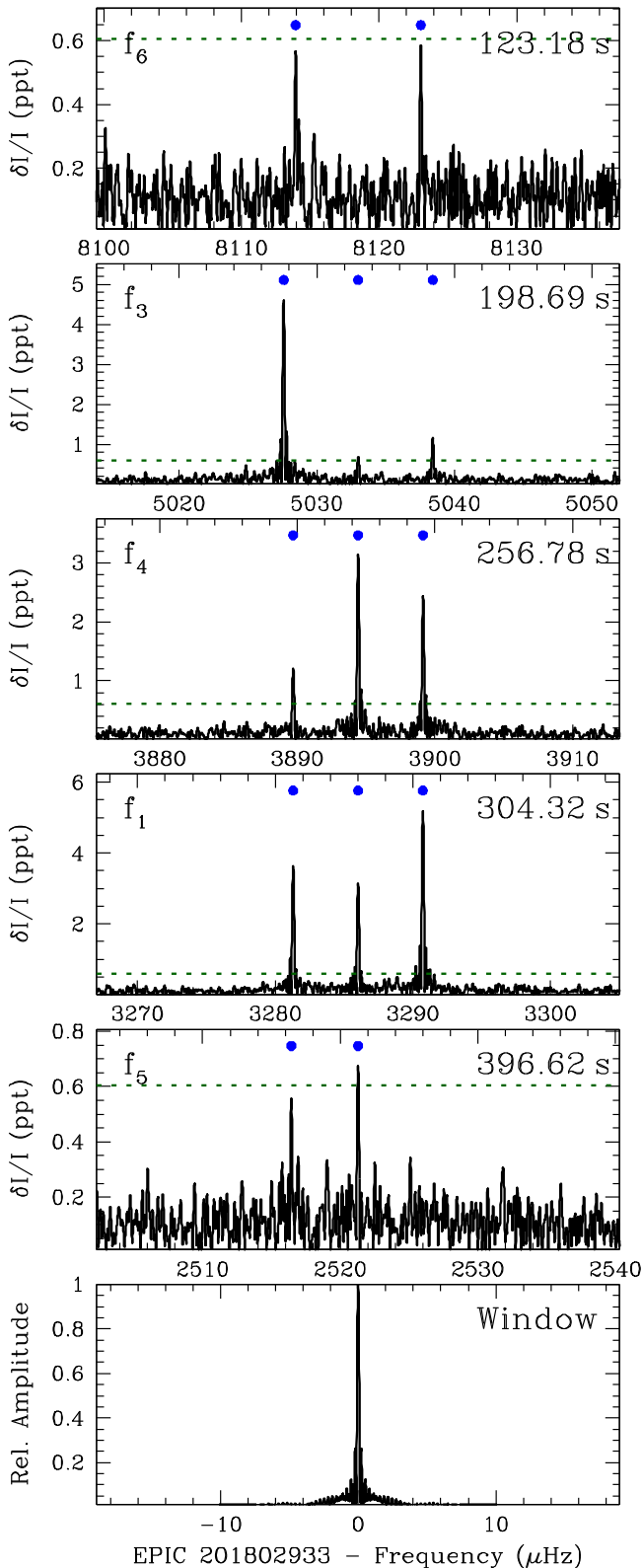[8] All reduced light curves are available online at http://www.k2wd.org.

Figure 1. Detailed look at the Fourier transform of EPIC 201802933 (SDSS J1151+0525, $K_{\rm p}$ = 17.7 mag), a new DAV discovered with *K2* and representative of most of the hot DAVs analyzed here. The green dotted line shows the 1% FAP (see text). The *K2* photometry features an exceptionally sharp spectral window (shown in the bottom panel), simplifying mode identification. All of the pulsations shown here are most simply interpreted as components of five different radial orders (k) of $\ell = 1$ dipole modes. The median frequency splitting of the five dipole modes is $\delta f = 4.7\ \mu$Hz, which corresponds to a roughly 1.3 day rotation period (see Section 7).

4. Follow-up WHT and SOAR Spectroscopy

We complemented our space-based photometry of these 27 DAVs by determining their atmospheric parameters based on model-atmosphere fits to follow-up spectroscopy obtained from two 4 m class, ground-based facilities. We detail these spectroscopic observations and their resultant fits in Table 3. Our spectra were obtained, reduced, and fit in a homogeneous way to minimize systematics.

DAVs in the original *Kepler* mission field are at such high declination ($\delta > +39$ deg) that they can only be observed from the northern hemisphere, so we used the Intermediate-dispersion Spectrograph and Imaging System (ISIS) instrument mounted on the 4.2 m William Herschel Telescope (WHT) on the island of La Palma for these five northern DAVs. Their spectra were taken with a 600 line mm^{-1} grating and cover roughly 3800–5100 Å at roughly 2.0 Å resolution using the blue arm of ISIS. A complete journal of observations for these five DAVs is detailed in Greiss et al. (2016), and we only list in Table 3 the night for which most observations were obtained.

All *K2* fields lie along the ecliptic, so we obtained spectroscopy of all *K2* DAVs with the Goodman spectrograph (Clemens et al. 2004) mounted on the 4.1 m Southern Astrophysical Research (SOAR) telescope on Cerro Pachón in Chile. Using a high-throughput 930 line mm^{-1} grating, we adopted grating and camera angles (13 degrees and 24 degrees, respectively) that yield wavelength coverage from roughly 3600–5200 Å. With 2×2 binning, our dispersion is 0.84 Å pixel^{-1}. To capture as much flux as possible, we use a 3″ slit, so our spectral resolution is seeing limited, roughly 3 Å in 1″0 seeing and roughly 4 Å in 1″4 seeing.

For each DAV, we obtained a series of consecutive spectra covering at least two cycles of the highest-amplitude pulsation, as derived from the *Kepler* photometry. We also made attempts to observe our targets at minimum airmass, which we list in Table 3, along with the mean seeing during the observations, measured from the mean FWHM in the spatial direction of the two-dimensional spectra.

All of our spectra were debiased and flat-fielded using a quartz lamp, using standard STARLINK routines (Currie et al. 2014). They were optimally extracted (Horne 1986) using the software PAMELA. We then used MOLLY (Marsh 1989) to wavelength calibrate, apply a heliocentric correction, and perform a final weighted average of the one-dimensional (1D) spectra. We flux-calibrated each spectrum to a spectrophotometric standard observed using the same setup at a similar airmass, and used a scalar to normalize this final spectrum to the g magnitude from any of the SDSS, VST/ATLAS, APASS, or KIS photometric surveys in order to correct its final absolute flux calibration.

We use the mean seeing to compute the spectral resolution, which informs the S/N per resolution element of the final spectra; the values listed in Table 3 were computed using a 100 Å wide region of the continuum centered at 4600 Å.

We fit the six Balmer lines, Hβ–H9, of our final 1D spectra to pure-hydrogen, 1D model atmospheres for white dwarfs. In short, the models employ the latest treatment of Stark broadening, as well as the ML2/$\alpha = 0.8$ prescription of the mixing-length theory. A full description of the models and fitting procedures is contained in Tremblay et al. (2011). For each individual DAV, the models were convolved to match the mean seeing during the observations.

Table 3
Follow-up Spectroscopy of the First 27 Pulsating DA White Dwarfs Observed by *Kepler* and *K2*

KIC/EPIC	g (mag)	Facility, Night of	Exp. (s)	Seeing (″)	Airm. Avg.	S/N	$T_{\rm eff}-1$D (K)	$\Delta T_{\rm eff}$ (K)	$\log g - 1$D (cgs)	$\Delta \log g$ (cgs)	$T_{\rm eff}-3$D (K)	$\log g - 3$D (cgs)	$M_{\rm WD}$ ($M_\odot$)
4357037	18.2	WHT, 2013 Jun 06	3 × 1200	0.9	1.07	77	12750	240	8.020	0.062	12650	8.013	0.62
4552982†	17.7	WHT, 2014 July 25	5 × 1200	0.7	1.06	76	11240	160	8.280	0.053	10950	8.113	0.67
7594781	18.1	WHT, 2014 July 25	6 × 1800	0.8	1.11	70	12040	210	8.170	0.059	11730	8.107	0.67
10132702	19.0	WHT, 2013 Jun 06	3 × 1500	0.9	1.06	70	12220	240	8.170	0.072	11940	8.123	0.68
11911480	18.0	WHT, 2013 Jun 07	3 × 1200	1.0	1.22	68	11880	190	8.020	0.061	11580	7.959	0.58
60017836	13.3	SOAR, 2016 Jul 14	5 × 30	2.1	1.11	210	11280	140	8.144	0.040	10980	7.995	0.60
201355934	17.8	SOAR, 2017 Apr 20	5 × 300	1.2	1.13	73	12050	170	8.016	0.047	11770	7.972	0.59
201719578	18.1	SOAR, 2017 Apr 14	8 × 300	1.4	1.22	62	11390	150	8.068	0.047	11070	7.941	0.57
201730811	17.1	SOAR, 2015 Jan 28	4 × 420	1.0	1.24	139	12600	170	7.964	0.043	12480	7.956	0.58
201802933	17.6	SOAR, 2016 Feb 14	3 × 360	1.4	1.23	75	12530	180	8.136	0.046	12330	8.114	0.68
201806008†	14.9	SOAR, 2016 Jun 22	7 × 180	1.1	1.29	161	11200	140	8.182	0.040	10910	8.019	0.61
206212611	17.3	SOAR, 2016 Jul 14	3 × 300	1.4	1.07	77	11120	150	8.170	0.048	10830	7.999	0.60
210397465	17.6	SOAR, 2016 Sep 01	5 × 300	1.8	1.27	50	11520	160	7.782	0.054	11200	7.713	0.45
211596649	18.9	SOAR, 2017 Feb 28	7 × 600	1.8	1.22	51	11890	180	7.967	0.057	11600	7.913	0.56
211629697†	18.3	SOAR, 2016 Dec 27	13 × 420	2.6	1.29	71	10890	150	7.950	0.060	10600	7.772	0.48
211914185	18.8	SOAR, 2017 Jan 25	9 × 600	2.0	1.38	61	13620	380	8.437	0.058	13590	8.434	0.88
211916160	18.9	SOAR, 2017 Apr 21	10 × 480	1.2	1.60	56	11820	170	8.027	0.053	11510	7.958	0.58
211926430	17.6	SOAR, 2016 Dec 27	11 × 420	2.2	1.30	98	11740	160	8.065	0.045	11420	7.982	0.59
228682478	18.2	SOAR, 2016 Jan 08	4 × 600	1.3	1.28	99	12340	170	8.226	0.046	12070	8.184	0.72
229227292†	16.6	SOAR, 2016 Feb 14	6 × 180	1.2	1.20	103	11530	150	8.146	0.042	11210	8.028	0.62
229228364†	17.8	SOAR, 2016 Jul 05	8 × 420	1.9	1.06	147	11330	140	8.172	0.043	11030	8.026	0.62
220204626	18.4	SOAR, 2016 Jul 05	7 × 420	1.7	1.22	74	11940	250	8.255	0.061	11620	8.173	0.71
220258806	16.2	SOAR, 2016 Jul 14	3 × 180	2.1	1.18	134	12890	200	8.093	0.047	12800	8.086	0.66
220347759	17.6	SOAR, 2016 Jul 05	5 × 300	1.5	1.32	81	12860	200	8.087	0.047	12770	8.080	0.66
220453225†	17.9	SOAR, 2016 Jul 05	7 × 300	1.6	1.49	72	11540	160	8.153	0.045	11220	8.035	0.62
229228478	16.9	SOAR, 2014 Oct 13	6 × 180	1.3	1.19	75	12610	180	7.935	0.045	12500	7.929	0.57
229228480	18.8	SOAR, 2016 Aug 07	7 × 600	1.0	1.17	65	12640	190	8.202	0.047	12450	8.181	0.72

References. We use a "†" symbol to mark the first six outbursting white dwarfs (Bell et al. 2015, 2016, 2017; Hermes et al. 2015b).
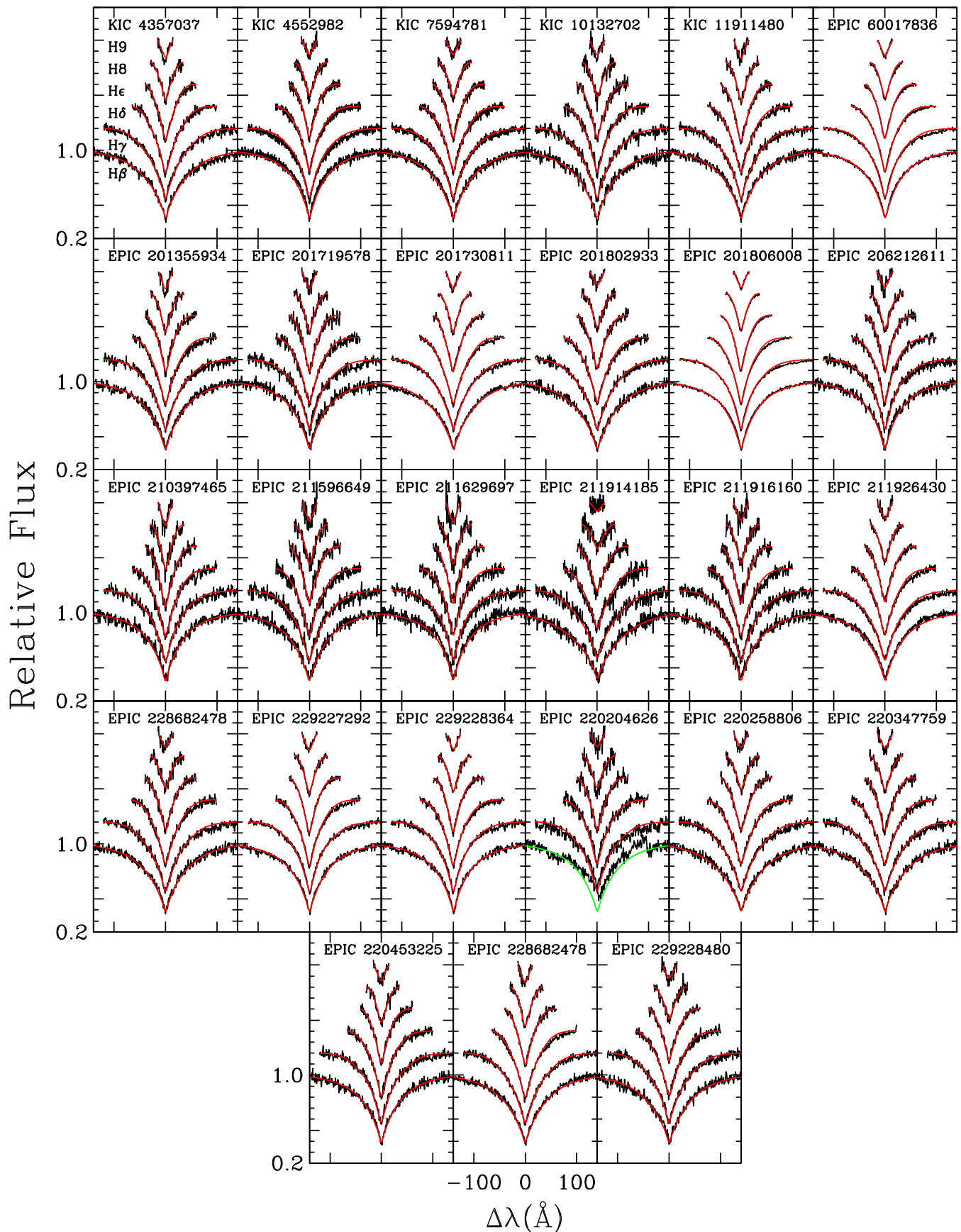
(This table is available in machine-readable form.)

Figure 2. Averaged, normalized spectra for the 27 DAVs observed through *K2* Campaign 8, overplotted with the best-fit atmospheric parameters detailed in Table 3. We observed the five DAVs from the original *Kepler* mission with the ISIS spectrograph on the 4.2 m William Herschel Telescope; all others were observed with the Goodman spectrograph on the 4.1 m SOAR telescope. Tremblay et al. (2011) describes the models and fitting procedures, which use ML2/$\alpha = 0.8$; atmospheric parameters have been corrected for the three-dimensional dependence of convection (Tremblay et al. 2013).
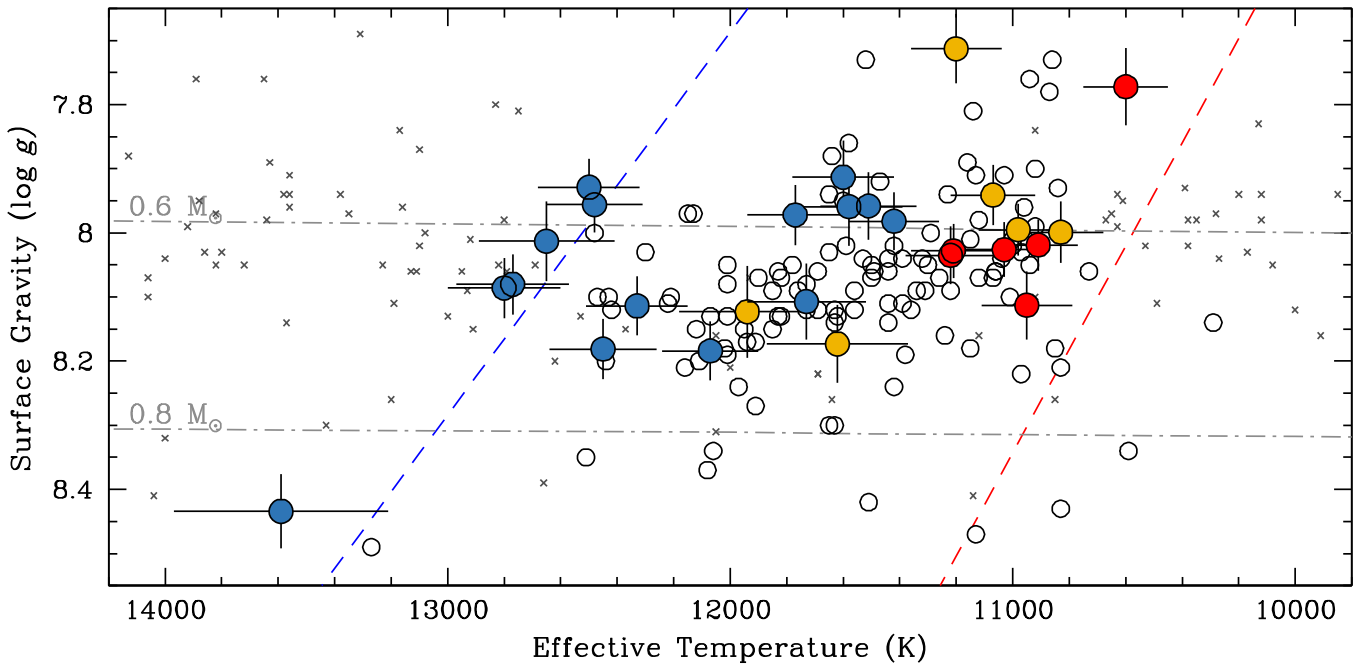
Figure 3. DAVs with *Kepler* data in the context of the empirical DAV instability strip, demarcated with the blue and red dashed lines most recently updated by Tremblay et al. (2015). We mark all DAVs with weighted mean pulsation periods shorter than 600 s in blue and those greater than 600 s in gold (see Section 6). Cool DAVs that show outbursts are marked in red (see Section 6). Known DAVs from ground-based observations are shown with open circles, and DAs not observed to vary to higher than 4 ppt are marked with gray crosses (Gianninas et al. 2011; Tremblay et al. 2011). All atmospheric parameters were analyzed with the same models, using ML2/α = 0.8, and corrected for the 3D dependence of convection (Tremblay et al. 2013). Dashed–dotted gray lines show the cooling tracks for 0.6 $M_\odot$ and 0.8 $M_\odot$ white dwarfs (Fontaine et al. 2001).

The 1D effective temperatures and surface gravities found from these fits are detailed in Table 3; the fits are visualized in Figure 2. We add in quadrature systematic uncertainties of 1.2% on the effective temperature and 0.038 dex on the surface gravity (Liebert et al. 2005). We use the analytic functions based on the three-dimensional (3D) convection simulations of Tremblay et al. (2013) to correct these 1D values to 3D atmospheric parameters, which we list in Table 3 as $T_{\rm eff} - 3D$ and $\log g - 3D$. We adopt these 3D-corrected atmospheric parameters as our estimates of the effective temperature and surface gravity of our 27 DAVs here, and use them in concert with the white dwarf models of Fontaine et al. (2001; which have thick hydrogen layers and are uniformly mixed, 50% carbon and 50% oxygen cores) to estimate the overall mass of our DAVs. Our overall mass estimates do not change by more than the adopted uncertainties (0.04 $M_\odot$ for all white dwarfs here) if we instead use the models of Renedo et al. (2010), which have more realistic carbon–oxygen profiles resulting from full evolutionary sequences.

Notably, two DAVs in our sample have line-of-sight dM companions, one of which strongly contaminates the Hβ line profiles. For this DAV (EPIC 220204626, SDSS J0111+0009), we omitted the Hβ line from our fits.

Our fitting methodology differs slightly from that adopted by Greiss et al. (2016) in that we fit the averaged spectrum rather than each spectrum individually, so our reported parameters are slightly different from those reported there but are still within the 1σ uncertainties. However, we note that the values for KIC 4357037 (KIS J1917+3927) were misreported in Greiss et al. (2016) and are corrected here.

We put our spectroscopic effective temperatures and surface gravities in the context of the empirical DAV instability strip in Figure 3; we show the empirical blue and red edges found by Tremblay et al. (2015). All atmospheric parameters, including literature DAVs and white dwarfs not observed to vary, were determined using the same 1D models using ML2/α = 0.8, and all were corrected to account for the 3D dependence of convection. Since *Kepler* is often more sensitive to lower-amplitude pulsations than instruments from the ground, it appears the empirical blue edge of the instability strip may need to be adjusted by roughly 200 K to hotter temperatures, but we leave that discussion to future analyses.

We adopt in Figure 3 a color code that we will use throughout the manuscript. We mark in blue all DAVs with a weighted mean period (WMP) shorter than 600 s (as described in more detail in Section 6), which cluster at the hotter (blue) half of the instability strip. We mark in gold all DAVs with a WMP exceeding 600 s. Finally, we mark in red the first six outbursting DAVs (Bell et al. 2017), all of which we mark in Table 3 with a "†" symbol. These outbursting DAVs are also all cooler than 11,300 K and exhibit stochastic, large-amplitude flux excursions we call outbursts.

Outbursts in the coolest DAVs were first discovered in the long-baseline monitoring of the *Kepler* spacecraft (Bell et al. 2015) and confirmed in a second DAV observed in *K2* Campaign 1 (Hermes et al. 2015b). A detailed discussion of this interesting new phenomenon is outside the scope of this paper, but we previously demonstrated that outbursts affect (and may be affected by) pulsations (Hermes et al. 2015b).

Interestingly, there are three *K2* pulsating white dwarfs near or even cooler than the first six outbursting DAVs. One of these
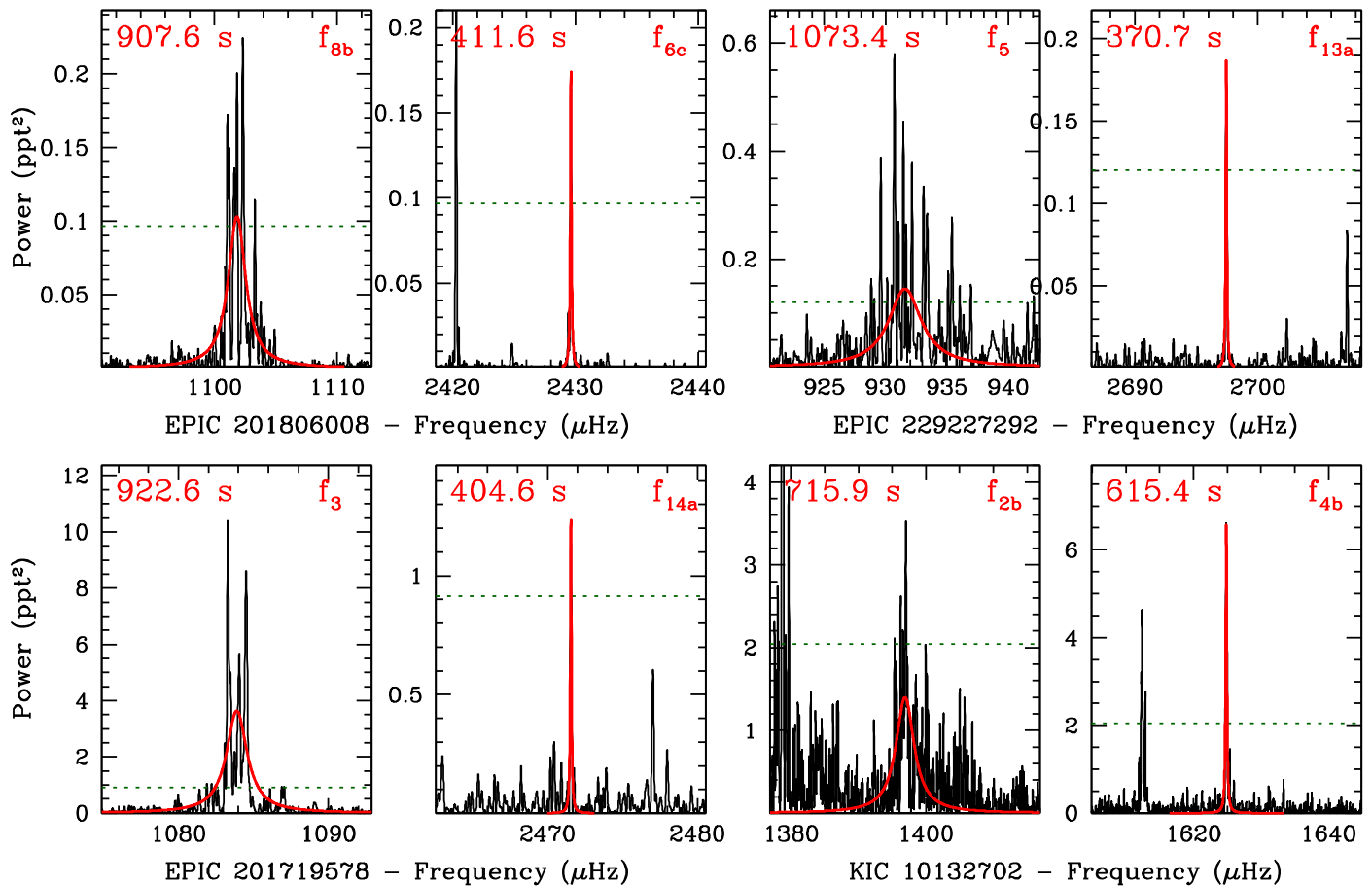
Figure 4. Detailed portions of the Fourier transforms of four DAVs observed with *K2* showing that pulsations with periods exceeding roughly 800 s (frequencies $<1250~\mu$Hz) have power broadly distributed outside the spectral window of the *Kepler* observations. For every DAV, we fit a Lorentzian to each independent mode, as described in Section 5. In the top left, we show two modes in EPIC 201806008 (PG 1149+058): f_{8b}, likely the $m = 0$ component of an $\ell = 2$ mode centered at 907.6 s, has power broadly distributed, with HWHM $= 0.868~\mu$Hz, whereas f_{6c}, the $m = +1$ component of the $\ell = 1$ mode centered at 412.40 s, has a sharp peak with HWHM $= 0.056~\mu$Hz. Similarly, in the top-right panels, we show two modes in EPIC 229227292 (ATLAS J1342−0735): the band of power centered at 1073.44 s, which has HWHM $= 1.632~\mu$Hz, is significantly broader than the $m = -1$ component of the $\ell = 1$ mode centered at 370.05 s. The bottom-left panels show a similar behavior in EPIC 201719578 (WD 1119+042): the 922.60 s mode in the same star has an HWHM of $0.836~\mu$Hz, whereas the 404.60 s mode has an HWHM of $0.045~\mu$Hz. Finally, we show KIC 10132702 (KIS J1913+4709) in the bottom-right panel, where the 715.86 s mode has an HWHM of $1.632~\mu$Hz, whereas the 615.44 s mode has an HWHM of $0.104~\mu$Hz. The *x*-axis (frequency) scales are identical for each star. The best fits for each mode are detailed in Table 5 and overplotted here; the HWHM of the Lorentzian fits to all 27 DAVs are shown in Figure 5.

three is GD 1212, which only has nine days of observations, so the limits on a lack of outbursts are not robust. GD 1212 was re-observed by *K2* for more than 75 days in Campaign 12 and will be analyzed in a future publication. We will discuss our insights into the evolution of white dwarfs through the DAV instability strip from *K2* in Section 6.

5. A Dichotomy of Mode Line Widths

Long-baseline *Kepler* photometry has opened an unprecedented window into the frequency and amplitude stability of DAVs. From early observations of the first DAV observed with *Kepler*, we noticed broad bands of power in the Fourier transform. Rather than just a small number of peaks, we saw a large number of peaks under a broad envelope; the envelope was significantly wider than the sharp spectral windows (Bell et al. 2015). We saw similarly broad power bands in another cool DAV, GD 1212, observed during an engineering test run for *K2* (Hermes et al. 2014). The broadly distributed power was reminiscent of the power spectra of stochastically driven

oscillations in the Sun or other solar-like oscillators (Chaplin & Miglio 2013). However, as noted in Bell et al. (2015), white dwarfs have a sound-crossing time orders of magnitude shorter than their observed pulsation periods, so these broad line widths cannot be related to stochastic driving.

Additionally, it became clear that not all white dwarfs with long-baseline, space-based observations showed such broad line widths. For example, we observed multiple DAVs with hotter effective temperatures and shorter-period pulsations that were completely coherent, within the uncertainties, over several months of *Kepler* observations (Greiss et al. 2014; Hermes et al. 2015a).

Within the larger sample of the first 27 DAVs, we noticed an emergent pattern: a dichotomy of mode line widths, even within the same star, delineated almost entirely by the pulsation period. The shorter-period modes appear stable in phase, producing narrow peaks in the Fourier transform, while the longer-period modes are phase unstable, spreading their power over a broad band in the Fourier transform. To quantify this
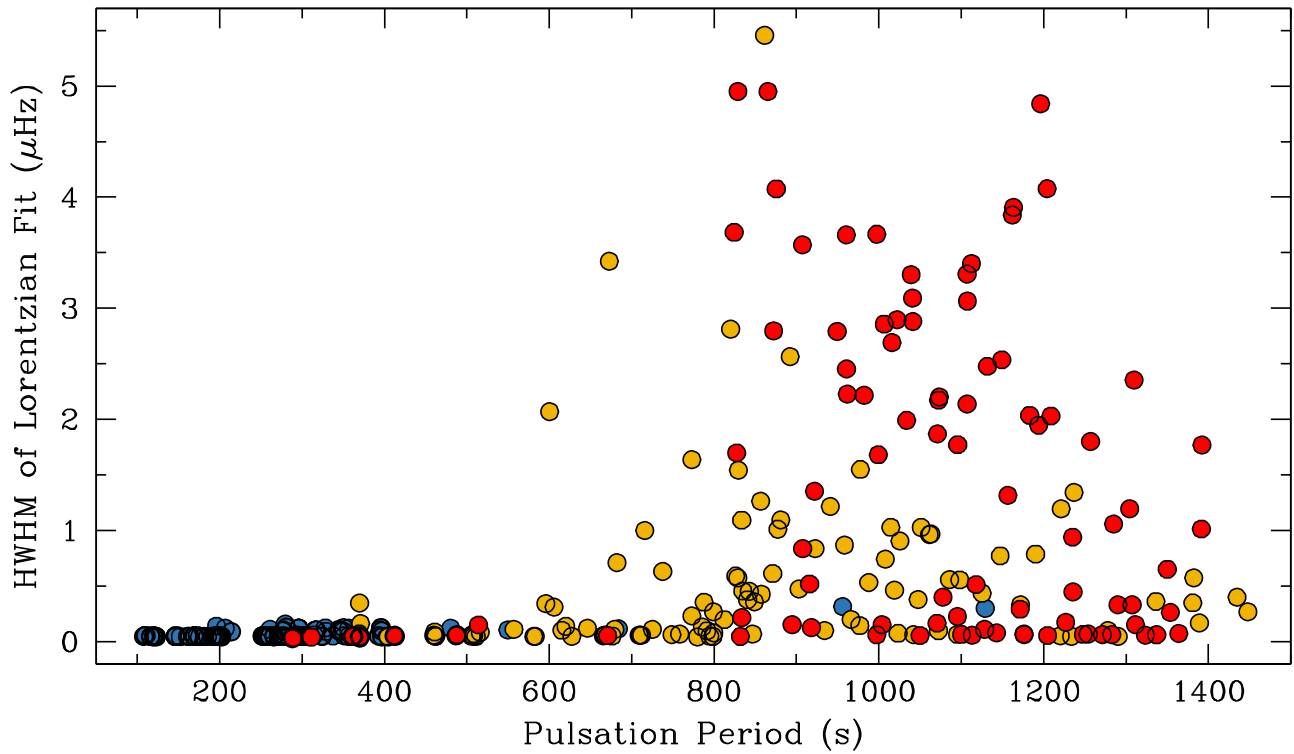
Figure 5. Half-width at half-maximum (HWHM) of Lorentzian functions fit to all significant peaks in the power spectra of the 27 DAVs observed through *K2* Campaign 8 by the *Kepler* space telescope; our procedure is described in Section 5. We use the same color classification as in Figure 3, where blue denotes objects with WMP < 600 s, gold with WMP > 600 s, and red those with outbursts (see Section 6). We excluded any nonlinear combination frequencies in this analysis. We see a sharp increase in HWHM at roughly 800 s, indicating that modes with relatively high radial order (k > 15 for ℓ = 1 modes) are not coherent in phase, similar in behavior to stochastically excited pulsators. We save a discussion of the possible physical mechanisms behind this phenomenon for a future work (M. H. Montgomery et al. 2017, in preparation).

behavior, we fit Lorentzian envelopes to every significant pulsation period and compare the period determined to the half-width at half-maximum (HWHM, γ) of the Lorentzian fits. Motivated by Toutain & Appourchaux (1994), we fit each thicket of peaks in the power spectrum (the square of the Fourier transform) with the function

$$\text{Power} = \frac{A\gamma^2}{(\nu - \nu_0)^2 + \gamma^2} + B, \qquad (1)$$

where A represents the Lorentzian height, γ is the HWHM, ν_0 is the central frequency of the peak, and B represents a DC offset for the background, which we hold fixed for all modes in the same star as the median power of the entire power spectrum. We only fit the region within 5 μHz to each side of the highest-amplitude peak within each band of power; this highest peak defines our initial guess for the central frequency, and we use an initial guess for the HWHM of 0.2 μHz, roughly twice our typical frequency resolution.

We illustrate the nature of the dichotomy of the mode line widths in Figure 4. Here we show, for four different DAVs in our sample, two independent modes within the same star that are well-separated in period. In each case, the shorter-period modes have line widths roughly matching the spectral window of the observations, with HWHM ⩽ 0.1 μHz. All DAVs in Figure 4 were observed by the *Kepler* spacecraft for more than 78 days with a duty cycle exceeding 91%. We observe that modes exceeding roughly 800 s (with frequencies below

roughly 1250 μHz) have much broader HWHM, often exceeding 1 μHz.

These broad bands of power are most likely representative of a single mode that is unstable in phase, reminiscent of a damped harmonic oscillator. For example, in the top-left panels of Figure 4, we show two modes in EPIC 201806008 (PG 1149 +058), the second outbursting DAV discovered (Hermes et al. 2015b). The mode f_{6c} is the $m = +1$ component of the $\ell = 1$ mode centered at 412.40 s; the two other components are seen at a slightly lower frequency (we discuss this splitting in the context of rotation in Section 7). The HWHM of f_{6c} is consistent with the spectral window: $\gamma = 0.056$ μHz. At much lower frequency, we identify the mode f_{8b} as the likely $m = 0$ component of an $\ell = 2$ mode centered at 907.58 s. Its power is much more broadly distributed, with $\gamma = 0.868$ μHz, too narrow to encompass other normal modes of different degrees or radial orders, but much broader than the spectral window.

We extend this Lorentzian analysis of mode line widths to the entire sample of 27 DAVs in Figure 5, which shows the period and HWHM computed for every Lorentzian fit to all 225 significant pulsations (we exclude all nonlinear combination frequencies from Figure 5; see Section 6). We performed the same experiment by fitting Gaussians to each peak and obtained a nearly identical distribution, so our choice of function does not significantly alter our results.

We see a sharp increase in HWHM at roughly 800 s, indicating that modes with relatively high radial order (k > 15 for ℓ = 1 modes) are not phase coherent, exhibiting behavior
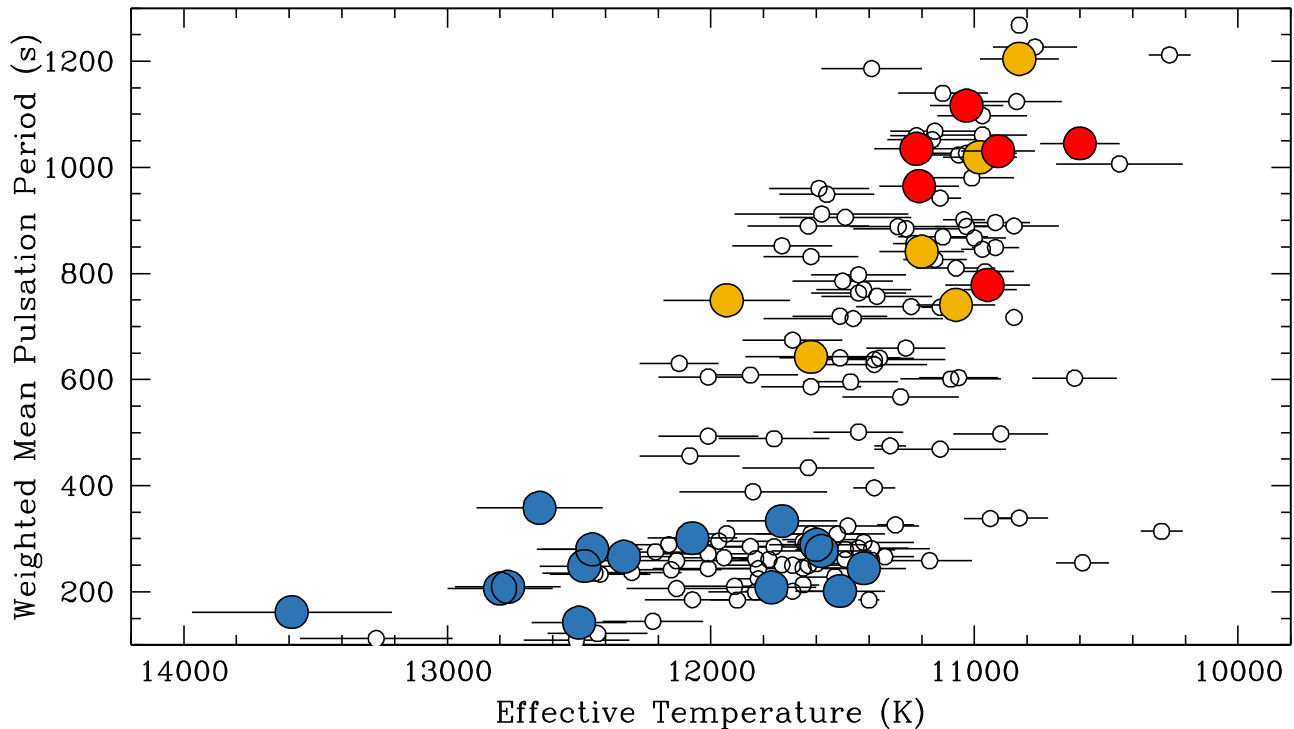
Figure 6. Following Clemens ([1993](#)), we plot the effective temperature vs. the weighted mean pulsation period (WMP) of each DAV analyzed here, using the same color classification used in Figure [3](#). We also show with white circles the 114 known DAVs from the literature with spectroscopy analyzed in the same way, also plotted in Figure [3](#).

similar to stochastically excited pulsators, although we do not believe the mode instability is related to stochastic driving.

One possibility is that the broad line widths arise from a process that has disrupted the phase coherence of the modes. In analogy with stochastically driven modes, we relate the observed mode line width (HWHM) to its lifetime (τ) via the relation $\tau = 2/(\pi\gamma)$ (Chaplin et al. [2009](#)). Doing so for the longer-period modes ($\gamma > 1\ \mu$Hz), we find mode lifetimes of order several days to weeks. This is comparable to the damping rates we expect for the roughly 1000 s $\ell = 1$ modes of typical pulsating white dwarfs (Goldreich & Wu [1999](#)). We will explore the possible physical mechanisms to explain these broad line widths in a future publication (M. H. Montgomery et al. 2017, in preparation).

Determining a pulsation period to use for the asteroseismology of the coolest DAVs with the longest-period modes is different from that for hot DAVs with narrow pulsation peaks that are determined via a linear least-squares fit and cleanly prewhitened. Therefore, for all modes with fitted HWHM exceeding $0.2\ \mu$Hz, we do not include their linear least-squares fits in Table [5](#), and instead only include the periods and amplitudes as determined from the Lorentzian fits in Table [5](#), with the period uncertainties computed from the HWHM.

6. Characteristics of the DAV Instability Strip

Pulsations in DAVs are excited by the "convective driving" mechanism, which is intimately tied to the surface hydrogen partial-ionization zone that develops as a white dwarf cools below roughly 13,000 K (Brickhill [1991](#); Wu & Goldreich [1999](#)). Driving is strongest for pulsations with periods nearest

to roughly 25 times the thermal timescale at the base of the convection zone (Goldreich & Wu [1999](#)).

By the time white dwarfs reach the DAV instability strip, their evolution is dominated by secular cooling. As they cool, the surface convection zone deepens, driving longer-period pulsations (e.g., Van Grootel et al. [2013](#)). These ensemble characteristics of the DAV instability strip, especially the lengthening of periods with cooler effective temperature, have been considered for decades (e.g., Clemens [1994](#)) and were most recently summarized observationally by Mukadam et al. ([2006](#)).

The most common way to visualize the increasing mode periods as DAVs cool is to compute the WMP of the significant pulsations (Clemens [1993](#)). The WMP is linearly weighted by the amplitude of each mode, such that $WMP = \sum_i P_i A_i / \sum_i A_i$, where P_i and A_i are the period and amplitude, respectively, of each significant independent pulsation detected (excluding nonlinear combination frequencies). We show the WMPs of all 27 DAVs observed by *Kepler* and *K2* so far in Figure [6](#), in addition to the WMP and temperatures of previously known DAVs with atmospheric parameters determined in the same way by Gianninas et al. ([2011](#)) and Tremblay et al. ([2011](#)).

Extensive coverage by the *Kepler* space telescope affords an even more nuanced exploration of the DAV instability strip. With our follow-up spectroscopic characterization of the first 27 DAVs observed with *Kepler* and *K2*, we can effectively put the evolutionary state of our pulsating white dwarfs into greater context. Figure [7](#) highlights five DAVs that are representative of the five different stages of evolution through the DAV instability strip, including color-coded Fourier transforms of each representative object. These data reveal important trends in the period and amplitude evolution of DAVs through the
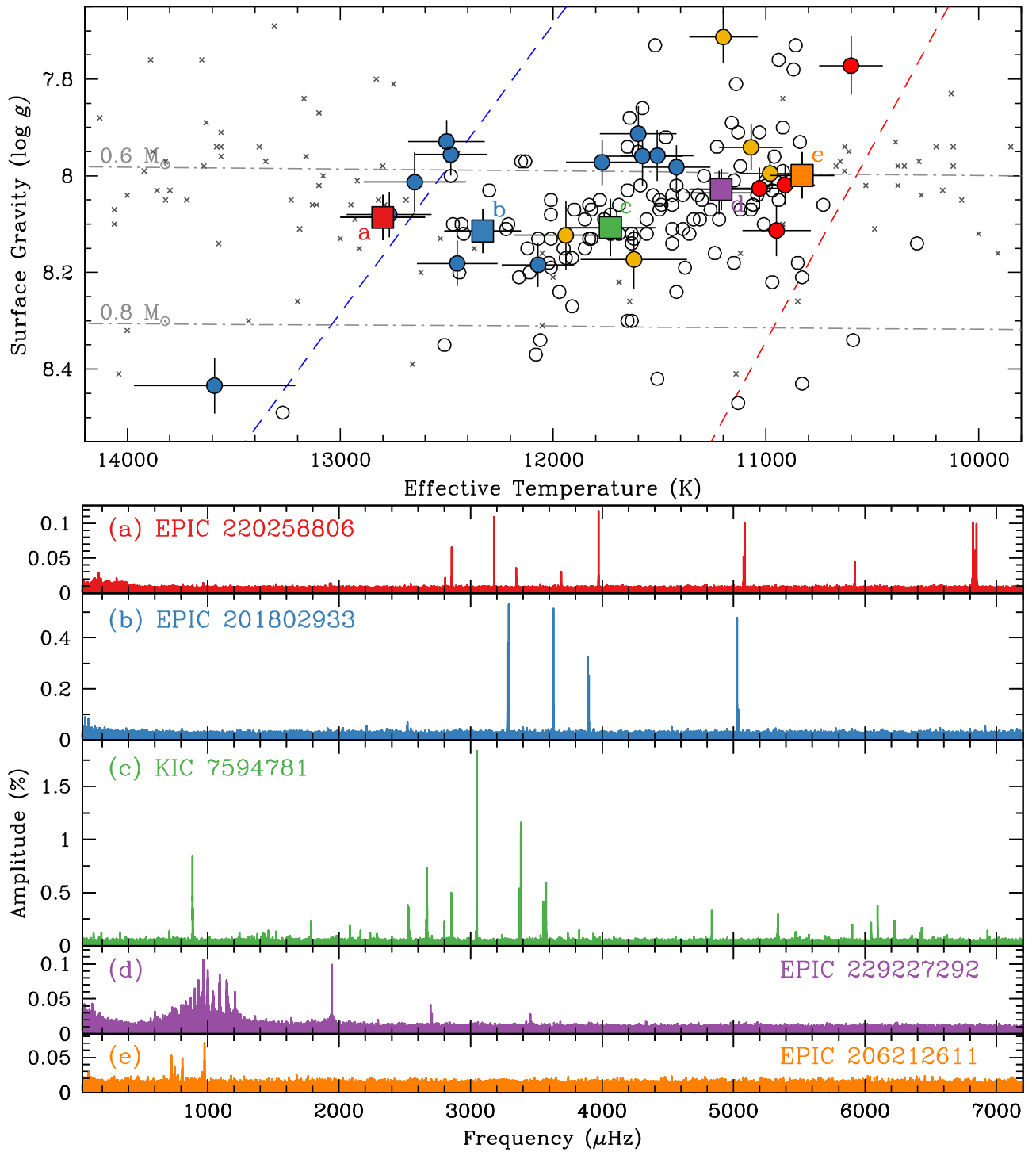
Figure 7. Top panel shows the same information as Figure 3 but color codes five representative stars in our sample to highlight the various phases of DAV cooling illuminated by *Kepler* observations so far, especially the pulsation period and amplitude evolution. In order of decreasing effective temperature, we highlight (a) EPIC 220258806 (SDSS J0106+0145), (b) EPIC 201802933 (SDSS J1151+0525), (c) KIC 7594781 (KIS J1908+4316), (d) EPIC 229227292 (ATLAS J1342−0735), and (e) EPIC 206212611 (SDSS J2220−0933). Fourier transforms of each are shown below with the same order and color coding, with amplitudes adjusted to reflect the target flux fractions found in Table 2. DAVs begin pulsating at the blue edge of the instability strip (a) with low-*k* (1 < *k* < 4) ℓ = 1, 2 modes from roughly 100–300 s and relatively low amplitudes (∼1 ppt). As they cool, (b) their convection zones deepen, driving longer-period (lower-frequency) pulsations with growing amplitudes. DAVs in the middle of the instability strip (c) have high-amplitude modes and the greatest number of nonlinear combination frequencies. As they cool further, (d) it appears common for DAVs to undergo aperiodic, sporadic outbursts; these DAVs tend to have many low-frequency modes excited in addition to one or several shorter-period, stable pulsations. Finally, a handful of DAVs have effective temperatures cooler than the outbursting DAVs but do not experience large-scale flux excursions (e); these coolest DAVs have the longest-period pulsations with relatively low amplitudes.

instability strip. Since there are likely mass-dependent effects, we describe this sequence for DAVs near the mean field white dwarf mass of 0.62 $M_\odot$, in order of hottest to coolest DAVs.

(a) DAVs begin pulsating at the blue edge of the instability strip with low-*k* (1 < *k* < 6) ℓ = 1, 2 modes from roughly 100–300 s and relatively low amplitudes (∼1 ppt). We

highlight in red in Figure 7 the hot (12,800 K) white dwarf EPIC 220258806 (SDSS J0106+0145) that appears to fall at the blue edge of the instability strip. This DAV has stable pulsations ranging from 116.28–356.14 s (WMP = 206.0 s), most of which are clearly identified as both $\ell = 1$ and $\ell = 2$ modes (see Table 5), although no modes have amplitudes in excess of roughly 1 ppt. The hottest DAVs in our sample have relatively low-amplitude modes. For example, the hottest DAV currently known is EPIC 211914185 (SDSS J0837+1856), which has just two relatively low-amplitude (1–3 ppt) dipole modes centered at 109.15 and 190.45 s (Hermes et al. 2017c). An example of a well-studied blue-edge DAV in this phase of evolution from ground-based observations is G226−29 (Kepler et al. 1995).

(b) As DAVs cool by a few hundred degrees from the blue edge, they retain relatively short-period pulsations but their observed amplitudes increase. For example, the 12,330 K EPIC 201802933 (SDSS J1151+0525) has amplitudes up to roughly 5 ppt with modes ranging from 123.11 to 396.62 s (WMP = 266.2 s). These low-k modes are expected to have extremely long mode lifetimes (Goldreich & Wu 1999), and most modes in these hot DAVs with mode periods shorter than 400 s appear coherent in phase. A well-known example of this phase of DAV evolution is G117-B15A (Robinson et al. 1995; Kepler et al. 2000).

(c) After DAVs cool by nearly 1000 K from the blue edge of the instability strip, their dominant pulsations exceed 300 s. DAVs in the middle of the instability strip tend to have very high-amplitude modes and the greatest number of nonlinear combination frequencies. For example, KIC 7594781 (KIS J1908+4316) is an 11,730 K white dwarf with the largest number of pulsation frequencies presented in our sample (WMP = 333.3 s). However, fewer than 10 of these frequencies of variability actually arise from unstable stellar oscillations—the rest are nonlinear combination frequencies (e.g., peaks corresponding to f_1+f_2 or $2f_1$), which arise from distortions of a linear pulsation signal caused by the changing convection zone of a DAV (Brickhill 1992; Montgomery 2005). These are not independent modes but rather artifacts of some nonlinear distortion in the outer layers of the star (Hermes et al. 2013).

Objects in the middle of the DAV instability strip represent a transition from hot, stable pulsations to cool DAVs with oscillations that are observed to change in frequency and/or amplitude on relatively short timescales. G29−38 is a prominent, long-studied example of a DAV representative of this phase in the middle of the instability strip (Kleinman et al. 1998).

(d) *Kepler* observations have now confirmed what appears to be a new phase in the evolution of DAVs as they approach the cool edge of the instability strip: aperiodic outbursts that increase the mean stellar flux by a few to 15%, last several hours, and recur sporadically on a timescale of days. Outbursts were first discovered in the original *Kepler* mission (Bell et al. 2015) and quickly confirmed in *K2* (Hermes et al. 2015b). Observational properties of the first six outbursting DAVs are detailed in Bell et al. (2017). Aside from many long-period pulsations, almost all of the outbursting DAVs observed by *Kepler* also show at least one and sometimes multiple shorter-period modes. Figure 7 highlights the Fourier transform of the 11,210 K outbursting DAV EPIC 229227292 (ATLAS J1342−0735), which is dominated by

pulsations from 827.7 to 1323.6 s (WMP = 964.5 s) but also shows significant periods centered around 514.1 s, 370.0 s, and 288.9 s (see Table 5). From the brightest outbursting DAV observed so far (PG 1149+058), we saw strong evidence that the pulsations respond to the outbursts (Hermes et al. 2015b).

(e) Finally, a handful of DAVs have effective temperatures as cool or cooler than the outbursting DAVs but do not experience large-scale flux excursions, suggesting that not all DAVs outburst at the cool edge of the instability strip. The coolest DAVs tend to have the longest-period pulsations with relatively low amplitudes. We highlight in Figure 7 the star EPIC 206212611 (SDSS J2220−0933), which is one of the coolest DAVs known, at 10,830 K. We do not detect any outbursts to a limit of 5.5%, following the methodology outlined in Bell et al. (2016). This DAV has modes from 1023.4 to 1381.2 s (WMP = 1204.4 s), all at relatively low amplitudes below 1 ppt.

7. Rotation Rates

The oscillations observed in white dwarfs are non-radial g-modes, which can be decomposed into spherical harmonics. Pulsations can thus be represented by three quantum numbers: the radial order (k, often expressed as n in other fields of asteroseismology), representing the number of radial nodes; the spherical degree (ℓ), representing the number of nodal lines expressed at the surface of the star; and the azimuthal order (m), representing the number of nodal lines in longitude at the surface of the star, ranging from $-\ell$ to ℓ.

Due to the strong geometric cancellation of higher-ℓ modes, we typically observe $\ell = 1$, 2 modes in white dwarfs. Rotation causes a lifting of degeneracy in the pulsation frequencies, causing a mode to separate into $2\ell + 1$ components in m (Unno et al. 1989). If all multiplets are present, this can result in triplets (for $\ell = 1$ modes) and quintuplets (for $\ell = 2$ modes) in the presence of slow rotation. This is corroborated by the many DAVs we observed with *Kepler* that show triplets and quintuplets of peaks evenly spaced in frequency: an exquisite example is the hot DBV PG 0112+104 (Hermes et al. 2017b). Observationally (and in contrast to solar-like oscillations), white dwarf pulsations do not partition mode energy equally into the various m components, such that the amplitudes of different m components for a given k, ℓ are not necessarily symmetric.

Still, we can use the clear patterns of frequency spacing in the Fourier transforms of our DAVs to say something about the rotation of these stellar remnants, summarized in Figure 8. This task is often complex from the ground due to diurnal aliasing, but the extended *Kepler* observations significantly simplifies mode identification and affords us the opportunity to probe internal rotation for 20 of the 27 DAVs we present here. For example, Figure 1 shows the five dipole ($\ell = 1$) modes in EPIC 201802933 (SDSS J1151+0525) identified from their split-tings. Evidence for splittings in other DAVs analyzed here can be found in Section 8.

To first order, the observed pulsation frequency splittings ($\delta\nu$) are related to the stellar rotation frequency (Ω) by the relation

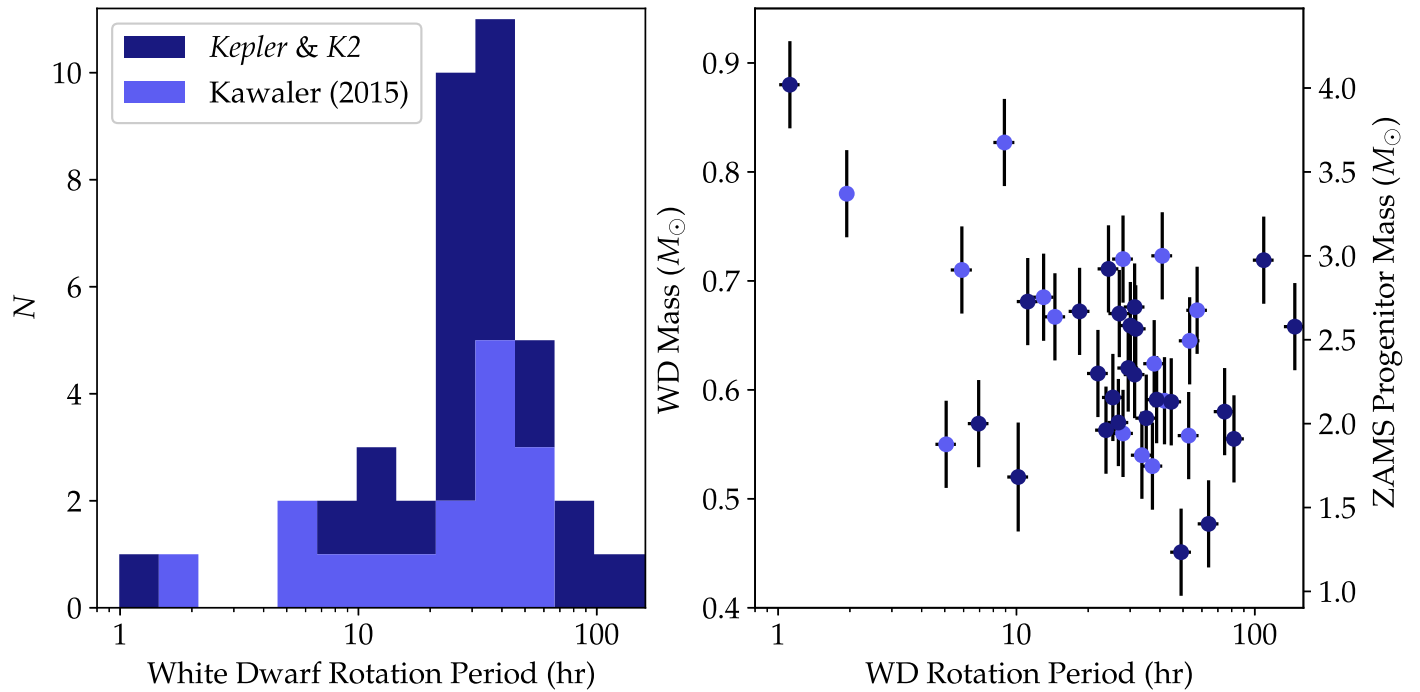$$\delta\nu = m(1 - C_{k,\ell})\Omega, \qquad (2)$$

Figure 8. We compare asteroseismically determined rotation periods for all known pulsating white dwarfs, detailed in Table 4. All white dwarfs presented here appear to be isolated stars, so these rotation periods should be representative of the endpoints of single-star evolution; we excluded the only known close binary (a WD+dM in a 6.9 hr orbit), EPIC 201730811 (SDSS J1136+0409, Hermes et al. 2015a). The left histogram shares the color coding of the right panel, which compares white dwarf rotation as a function of mass. Estimates of the ZAMS progenitor masses for each white dwarf are listed on the right axis. Notably, EPIC 211914185 (SDSS J0837+1856) is more massive ($0.88 \pm 0.03\,M_\odot$) and rotates faster (1.13 ± 0.02 hr) than any other pulsating white dwarf (Hermes et al. 2017c); we see evidence for a link between high mass and fast rotation, but require additional massive white dwarfs to confirm this trend.

where $C_{k,\ell}$ represents the effect of the Coriolis force on the pulsations, as formulated by Ledoux (1951). For high-k modes that approach the asymptotic, mode-independent limit for $\ell = 1$ modes, $C_{k,1} \rightarrow 0.50$. However, the low-k (especially $k < 10$) modes found in hot DAVs can suffer from strong mode-trapping effects that also significantly alter $C_{k,\ell}$ (e.g., Brassard et al. 1992). Theoretical DAV models in, for example, Romero et al. (2012), predict $C_{k,1}$ values typically ranging from roughly 0.45 to 0.49, with exceptions down to $C_{k,1} \sim 0.35$ for strongly trapped modes.

For the 20 DAVs here for which we have identified modes, all have at least one and many have multiple sets of $\ell = 1$ modes; the full catalog of asteroseismic rotation rates for white dwarfs is detailed in Table 4. To provide the best model-independent estimates for the rotation periods of the newly identified DAVs here, we compute the median frequency splitting of all identified $\ell = 1$ modes ($\delta\nu_{\ell=1}$), which we list in Table 4. We then hold fixed $C_{k,1} = 0.47$ and use $\delta\nu_{\ell=1}$ to estimate the DAV rotation period. We put these new DAV rotation periods in the context of all other white dwarfs with measured rotation periods from asteroseismology compiled by Kawaler (2015) in Figure 8. *Kepler* and *K2* have more than doubled the number of white dwarfs for which we have measured internal rotation from pulsations.

We note that it is necessary to perform a complete asteroseismic analysis in order to estimate the best values for $C_{k,\ell}$ for the pulsation modes presented here. This also affords us the opportunity to significantly improve constraints on the rotation period; the choice of $C_{k,\ell}$ for each mode dominates the uncertainty on the overall rotation period measured from

the frequency splittings, since mode trapping is very common. Given our method of uniformly adopting $C_{k,1} = 0.47$, we estimate that each rotation period has a systematic uncertainty of roughly 10%, though we note that $C_{k,\ell}$ cannot exceed 0.50.

Importantly, because we measured the atmospheric parameters of all DAVs observed with *Kepler* so far, we have for the first time a large enough sample to determine how rotation periods in white dwarfs differ as a function of the overall white dwarf mass. We see in Figure 8 suggestions of a trend of decreasing rotation period with increasing white dwarf mass. We also include on the right axis estimates for the ZAMS progenitor mass, calculated from the cluster-calibrated white dwarf initial-to-final-mass relation of Cummings et al. (2016) for progenitor stars with masses below $4.0\,M_\odot$.

A first-order linear fit to the white dwarf mass–rotation plot in the right panel of Figure 8 yields an estimate of the final white dwarf rotation rate as a function of progenitor mass: $P_{\rm rot} = ((2.36 \pm 0.14) - M_{\rm ZAMS})/(0.0024 \pm 0.0031)$, where $P_{\rm rot}$ is the final rotation period expressed in hours and $M_{\rm ZAMS}$ is the ZAMS progenitor mass in solar masses. This linear trend is not yet statistically significant; we are actively seeking more white dwarfs with masses exceeding $0.72\,M_\odot$ (which likely arise from $>3.0\,M_\odot$ ZAMS progenitors) to improve estimates of this relationship.

The mass distribution of white dwarfs with rotation periods measured from pulsations is very similar to the mass distribution of field white dwarfs determined by Tremblay et al. (2016). If we restrict our analysis to only white dwarfs within 1σ of the mean mass and standard deviation of field white dwarfs (i.e., nearly 70% of all field white dwarfs), we are

Table 4
Rotation Rates of Isolated White Dwarfs Determined via Asteroseismology

Star Name	R.A. and Decl. (J2000)	Class	$T_{\rm eff}$ − 3D (K)	WD Mass ($M_\odot$)	$\Delta M_{\rm WD}$ ($M_\odot$)	Prog. Mass ($M_\odot$)	$\Delta M_{\rm Prog.}$ ($M_\odot$)	$\delta\nu_{\ell=1}$ (μHz)	$P_{\rm rot}$ (hr)	Ref.
Literature Values for All Classes of Pulsating White Dwarfs Compiled by Kawaler (2015)
Ross 548	01 36 13.58 − 11 20 32.7	DAV	12300	0.62	0.04	2.36	0.47	⋯	37.8	1
HL Tau 76	04 18 56.63 + 27 17 48.5	DAV	11470	0.56	0.04	1.93	0.44	⋯	52.8	2
HS 0507 + 0434	05 10 13.94 + 04 38 38.4	DAV	12010	0.72	0.04	3.00	0.52	3.6	40.9	3
KUV11370 + 4222	11 39 41.42 + 42 05 18.7	DAV	11940	0.71	0.04	2.92	0.51	25.0	5.9	4
GD 154	13 09 57.69 + 35 09 47.1	DAV	11120	0.65	0.04	2.49	0.48	2.8	53.3	5
LP 133 − 144	13 51 20.24 + 54 57 42.6	DAV	12150	0.59	0.04	2.13	0.45	⋯	41.8	6
GD 165	14 24 39.14 + 09 17 14.0	DAV	12220	0.67	0.04	2.68	0.50	⋯	57.3	1
L19-2	14 33 07.60 − 81 20 14.5	DAV	12070	0.69	0.04	2.75	0.50	13.0	13.0	7
SDSS J1612 + 0830	16 12 18.08 + 08 30 28.1	DAV	11810	0.78	0.04	3.50	0.55	75.6	1.9	8
G226-29	16 48 25.64 + 59 03 22.7	DAV	12510	0.83	0.04	3.68	0.57	⋯	8.9	9
G185-32	19 37 13.68 + 27 43 18.7	DAV	12470	0.67	0.04	2.64	0.49	⋯	14.5	10
PG 0122 + 200	01 25 22.52 + 20 17 56.8	DOV	80000	0.53	0.04	1.75	0.42	3.7	37.2	11
NGC 1501	04 06 59.39 + 60 55 14.4	DOV	134000	0.56	0.04	1.94	0.44	⋯	28.0	12
PG 1159 − 035	12 01 45.97 − 03 45 40.6	DOV	140000	0.54	0.04	1.81	0.43	⋯	33.6	13
RX J2117.1 + 3412	21 17 08.28 + 34 12 27.5	DOV	170000	0.72	0.04	2.98	0.52	⋯	28.0	14
PG 2131 + 066	21 34 08.23 + 06 50 57.4	DOV	95000	0.55	0.04	1.88	0.43	⋯	5.1	15
KIC 8626021	19 29 04.69 + 44 47 09.7	DBV	30000	0.59	0.04	2.10	0.45	3.3	44.6	16
EPIC 220670436	01 14 37.66 + 10 41 04.8	DBV	31300	0.52	0.04	1.68	0.42	15.4	10.2	17
Rotation Rates from DAVs Analyzed Here
KIC 4357037	19 17 19.20 + 39 27 19.1	DAV	12650	0.62	0.04	2.30	0.47	6.7	22.0	0
KIC 4552982	19 16 43.83 + 39 38 49.7	DAV	10950	0.67	0.04	2.67	0.50	8.0	18.4	18
KIC 7594781	19 08 35.88 + 43 16 42.4	DAV	11730	0.67	0.04	2.66	0.49	5.5	26.8	0
KIC 10132702	19 13 40.89 + 47 09 31.3	DAV	11940	0.68	0.04	2.73	0.50	13.2	11.2	0
KIC 11911480	19 20 24.90 + 50 17 21.3	DAV	11580	0.58	0.04	2.07	0.45	1.97	74.7	19
EPIC 60017836	23 38 50.74 − 07 41 19.9	DAV	10980	0.57	0.04	2.00	0.44	21.2	6.9	0
EPIC 201719578	11 22 21.10 + 03 58 22.4	DAV	11070	0.57	0.04	2.01	0.44	5.5	26.8	0
EPIC 201730811	11 36 55.16 + 04 09 52.8	DAV	12480	0.58	0.04	2.08	0.45	56.7	2.6	20
EPIC 201802933	11 51 26.15 + 05 25 12.9	DAV	12330	0.68	0.04	2.69	0.50	4.7	31.3	0
EPIC 201806008	11 51 54.20 + 05 28 39.8	DAV	10910	0.61	0.04	2.29	0.47	4.7	31.3	0
EPIC 210397465	03 58 24.23 + 13 24 30.8	DAV	11200	0.45	0.04	1.23	0.38	3.0	49.1	0
EPIC 211596649	08 32 03.98 + 14 29 42.4	DAV	11600	0.56	0.04	1.91	0.44	1.8	81.8	0
EPIC 211629697	08 40 54.14 + 14 57 09.0	DAV	10600	0.48	0.04	1.40	0.40	2.3	64.0	0
EPIC 211914185	08 37 02.16 + 18 56 13.4	DAV	13590	0.88	0.04	4.02	0.60	131.6	1.1	21
EPIC 211926430	09 00 41.08 + 19 07 14.4	DAV	11420	0.59	0.04	2.16	0.46	5.8	25.4	0
EPIC 228682478	08 40 27.84 + 13 20 10.0	DAV	12070	0.72	0.04	2.97	0.52	1.4	109.1	0
EPIC 229227292	13 42 11.62 − 07 35 40.1	DAV	11210	0.62	0.04	2.33	0.47	5.0	29.4	0
EPIC 220204626	01 11 23.89 + 00 09 35.2	DAV	11620	0.71	0.04	2.92	0.51	6.1	24.3	0
EPIC 220258806	01 06 37.03 + 01 45 03.0	DAV	12800	0.66	0.04	2.58	0.49	4.9	30.0	0
EPIC 220347759	00 51 24.25 + 03 39 03.8	DAV	12770	0.66	0.04	2.56	0.49	4.7	31.7	0

References. (0) This work; (1) Giammichele et al. (2016); (2) Dolez et al. (2006); (3) Fu et al. (2013); (4) Su et al. (2014); (5) Pfeiffer et al. (1996); (6) Bognár et al. (2016); (7) Bradley (2001); (8) Castanheira et al. (2013); (9) Kepler et al. (1995); (10) Pech & Vauclair (2006); (11) Fu et al. (2007); (12) Bond et al. (1996); (13) Charpinet et al. (2009); (14) Vauclair et al. (2002); (15) Kawaler et al. (1995); (16) Østensen et al. (2011); (17) Hermes et al. (2017b); (18) Bell et al. (2015); (19) Greiss et al. (2014); (20) Hermes et al. (2015a)—excluded from Figure 8 since the white dwarf is in a close, post-common-envelope binary; (21) Hermes et al. (2017c).

left with 34 pulsating white dwarfs with masses from 0.51 to 0.73 $M_\odot$ which have a mean rotation period of 35 hr with a standard deviation of 28 hr (35 ± 28 hr). The mean rotation period is essentially the same if we break the subsample into progenitor ZAMS masses spanning 1.7–2.0 $M_\odot$ (35 ± 23 hr), 2.0–2.5 $M_\odot$ (32 ± 18 hr), and 2.5–3.0 $M_\odot$ (32 ± 25 hr). However, the small sample of three massive white dwarfs, which evolved from 3.5 to 4.0 $M_\odot$ progenitors, appears to rotate significantly faster, at 4.0 ± 3.5 hr. This is visualized in Figure 9.

The original *Kepler* mission yielded exceptional insight into the rotational evolution of stars at most phases of stellar evolution (Aerts 2015), and now we can provide final boundary conditions on the question of internal angular momentum evolution in isolated stars. For example, *Kepler* data have been especially effective at illuminating differential rotation and angular momentum evolution in 1.0–2.0 $M_\odot$ first-ascent red giants (e.g., Mosser et al. 2012), where it was found that their cores are rotating roughly 10 times faster than their envelopes. Still, this is an order of magnitude slower than expected after accounting for all hypothesized angular momentum transport processes (e.g., Marques et al. 2013; Cantiello et al. 2014). Moving farther along the giant branch, *Kepler* has shown that 2.2–2.9 $M_\odot$ core-helium-burning secondary clump giants do
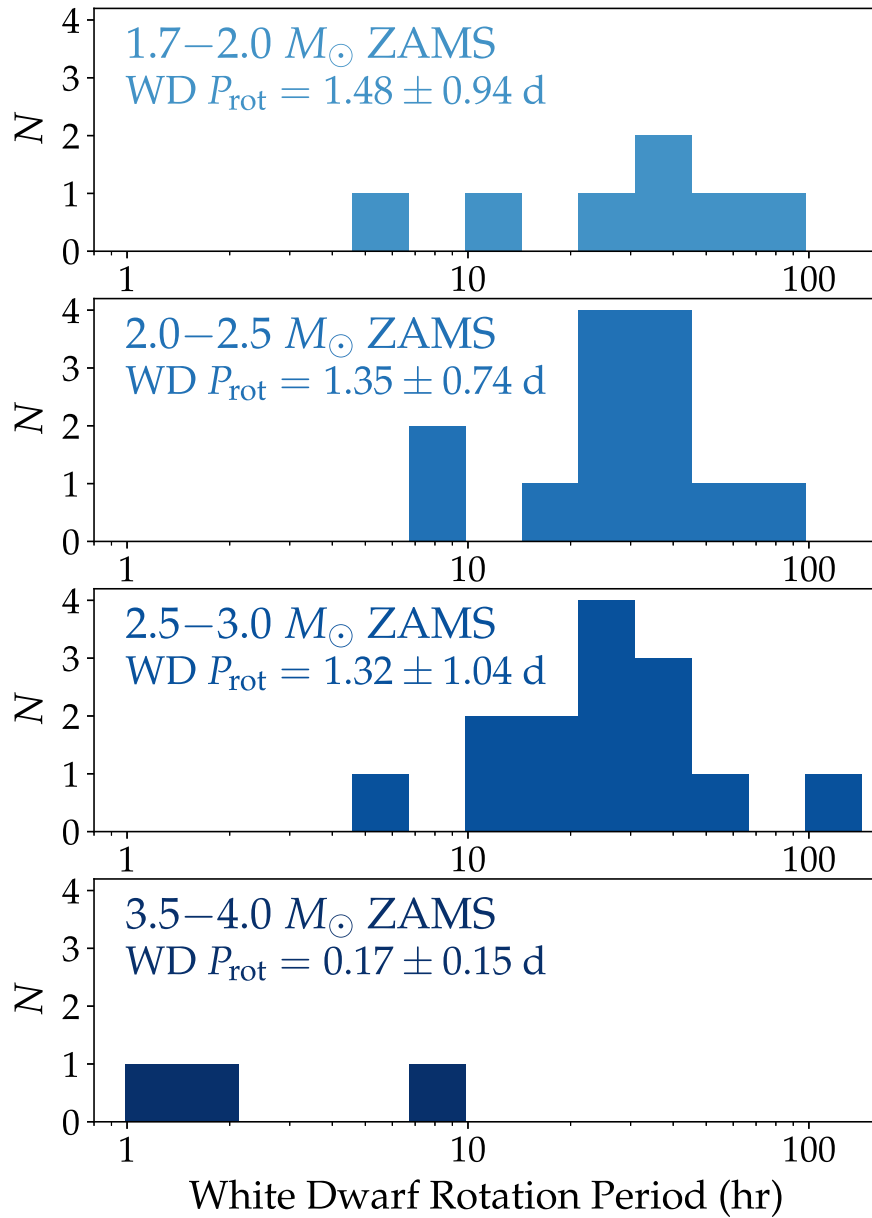
Figure 9. Rotation rates of pulsating, apparently isolated white dwarfs as a function of initial stellar mass, using the cluster-calibrated IFMR from Cummings et al. (2016). The 34 pulsating white dwarfs with masses from 0.51 to 0.73 $M_\odot$ (which descended from roughly 1.7 to 3.0 $M_\odot$ ZAMS stars) all have a mean rotation period of roughly 35 hr regardless of binning, but more massive white dwarfs (>0.75 $M_\odot$, which descended from >3.5 $M_\odot$ ZAMS stars) appear to rotate systematically faster.

not have as much radial differential rotation and have cores rotating at roughly 30–100 days (e.g., Deheuvels et al. 2015).

For decades, we have known that white dwarfs have relatively slow rotation, given that their surface rotation velocities usually do not exceed upper limits of 15 km s^{-1}, corresponding to periods longer than several hours (Koester et al. 1998). This is surprising: if we completely conserve the angular momentum of a 3.0 $M_\odot$ main-sequence star with an initial rotation period of 10 hr, its white dwarf remnant would be rotating faster than a few minutes (Kawaler 2004). We establish here that the majority of isolated descendants of 1.7–3.0 $M_\odot$ ZAMS progenitors rotate at 1.5 days, with a narrow dispersion between 0.5 and 2.2 days at the conclusion of their evolution. We note that we are sensitive to rotation periods longer than 15 days given our frequency resolution, but

the longest rotation period we measure is 109.1 hr (roughly 4.5 days) in EPIC 228682478.

8. Notes on Individual Objects

KIC 4357037 (KIS J1917+3927): With "only" 36.3 days of nearly uninterrupted *Kepler* observations, this is one of our shortest data sets, but still the data reveal seven independent pulsations, five of which we identify as $\ell = 1$ modes; we show in Figure 10 the two highest-amplitude modes, f_1 and f_2. As noted in Section 4, the atmospheric parameters for this object were misreported in Greiss et al. (2016), but are corrected here and find $T_{\rm eff} = 12{,}650$ K. Most periods we observe are in line with such a hot DAV, with the identified $\ell = 1$ modes spanning 214.40–396.70 s. However, there are several long-period
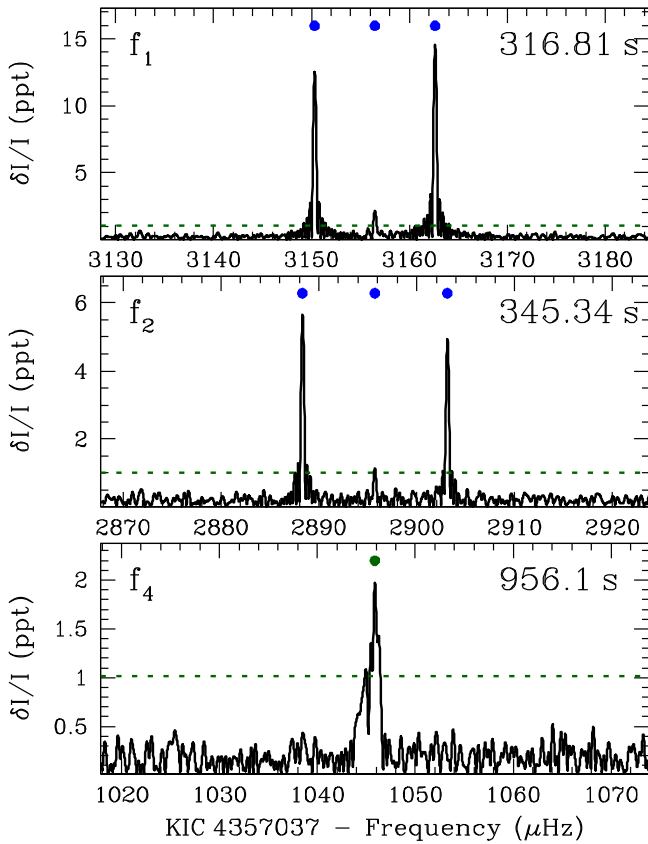
Figure 10. Highest-amplitude modes in KIC 4357037 (KIS J1917+3927), f_1 and f_2 ($\ell = 1$ modes marked with blue dots), illuminate the median $\ell = 1$ splitting of 6.8 μHz, corresponding to a 22.0 hr rotation period. We could not identify the longest-period mode also present in this star at 956.11 s (unidentified modes marked with green dots), which has a considerably broader line width than the shorter-period modes.

Figure 11. We show two modes in KIC 7594781 (KIS J1908+4316) which share the median $\ell = 1$ splitting of 5.5 μHz, suggesting a rotation period of 26.8 hr. This DAV has a broadened long-period mode at f_3 (1129.19 s), which appears in many of the nonlinear combination frequencies (Table 5).

modes that do not appear to be nonlinear difference frequencies, at 549.72 and 956.11 s. The latter mode at 956.11 s (bottom panel of Figure 10) is significantly broader than the spectral window, with HWHM = 0.318 μHz, suggesting that it is an independent mode in the star, given its position in Figure 5. It is at a much longer period than typically observed in such a hot DAV, posing an interesting question of how it is excited at the same time as other modes with three times shorter periods.

KIC 4552982 (KIS J1916+3938): This was the first DAV discovered in the original *Kepler* mission field and has the longest pseudo-continuous light curve of any pulsating white dwarf ever recorded, spanning more than 1.5 years. Our analysis here is focused on the HWHM of the modes present, and thus only includes roughly three months of data from Q12, to remain consistent with the frequency resolution of the other DAVs analyzed here. A more detailed light curve analysis, including discussion of the mean period spacing and results from Lorentzian fits to the full *Kepler* data set, can be found in Bell et al. (2015). The triplet at f_1 remains the only mode we have identified in this DAV; the large amplitude of this coherent mode at f_1 drives down the WMP of this DAV to 750.4 s, which we report from the period list of Bell et al. (2015). Our rotation rate differs slightly from that reported by Bell et al. (2015) since we adopt a lower assumed value for $C_{k,\ell}$.

KIC 7594781 (KIS J1908+4316): This DAV has a relatively short data set, with just 31.8 days of observations in Q16.2. We identify three modes in the star as $\ell = 1$ with a median splitting of 5.5 μHz, two of which are shown in Figure 11, suggesting a rotation period of 26.8 hr. Such a rotation rate would yield $\ell = 2$ splittings of roughly 8.6 μHz, so we suggest that f_1 may be an $\ell = 2$ mode, although the data are not definitive. As with KIC 4357037, there is a much longer period, highly broadened mode, here at 1129.19 s. Interestingly, this mode, f_3, combines with many other modes in the star to give rise to most of the 14 nonlinear combination frequencies present. When f_3 combines with other modes, its unique line width is reproduced; for this reason, although we could not identify any suitable combinations, we caution that f_4 may not be an independent mode in the star but could possibly be a combination frequency of f_3 in some way given the shape of f_4. Interestingly, f_3 is relatively stable in amplitude but changing rapidly in frequency. Its frequency in the first five days of data is relatively stable at 885.243 ± 0.057 μHz (7.08 ± 0.32 ppt), but its power in the last five days of *Kepler* data less than 27 days later had almost completely moved to 888.285 ± 0.067 μHz (6.14 ± 0.32 ppt). There is still much to be learned about the causes of short-term frequency, amplitude, and phase instability in white dwarf pulsations from further analysis of this *Kepler* data—nonlinear mode coupling appears to be the only way to explain how white dwarf pulsations can change character so rapidly (e.g., Zong et al. 2016).
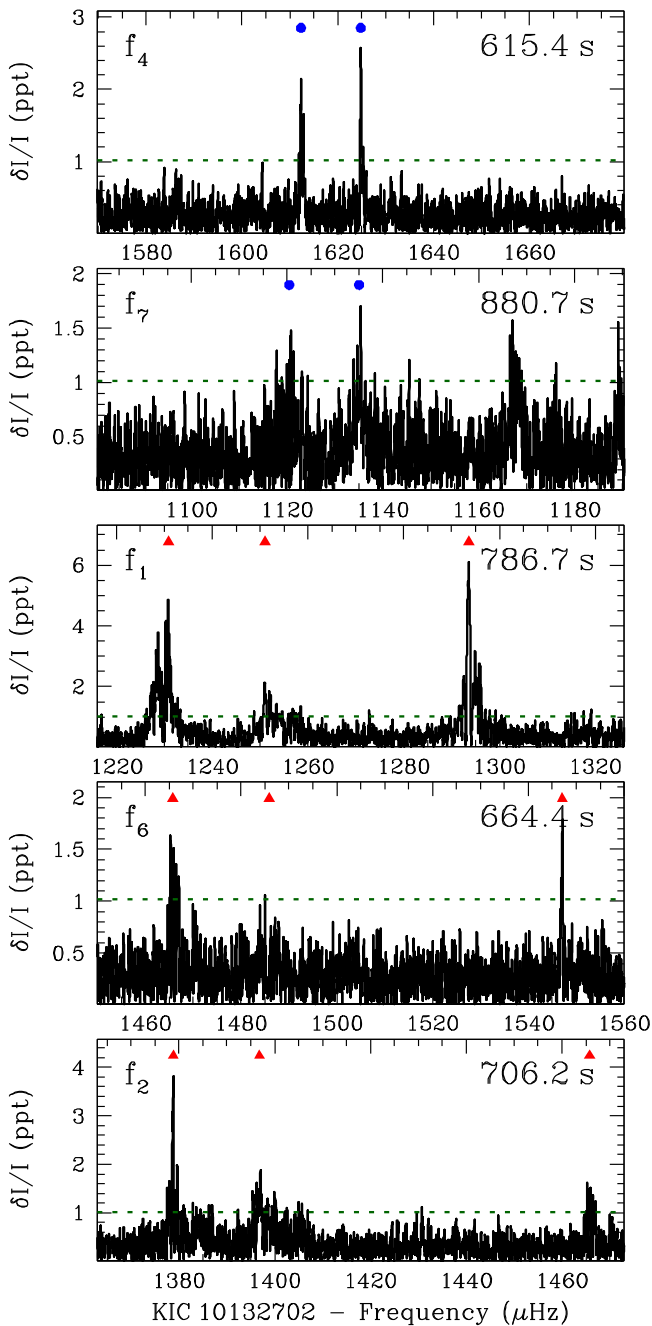
Figure 12. We show several components of $\ell = 1$ modes (marked with blue dots) and $\ell = 2$ modes (red triangles) in KIC 10132702 (KIS J1913+4709). The top two panels highlight the two dipole modes, with a median $\ell = 1$ splitting of 13.5 μHz. We also show what we have identified as three different quadrupole modes, with a median $\ell = 2$ splitting of 21.3 μHz. Our tentative m identification for these modes is detailed in Table 5. Both sets of splittings suggest a rotation period of roughly 11.2 hr.

Figure 13. We show one $\ell = 1$ mode (marked with blue dots) and three $\ell = 2$ modes (red triangles) in GD 1212. The dipole mode has an $\ell = 1$ splitting of 21.3 μHz, and our three different quadrupole modes have a median $\ell = 2$ splitting of 33.7 μHz. Our tentative m identification for these modes is detailed in Table 5. Both sets of splittings are self-consistent and reveal a rotation period of roughly 6.9 hr.

KIC 10132702 (KIS J1913+4709): We are able to identify seven of the eight independent modes in this DAV, five of which are shown in Figure 12. The periods span roughly 461.1–977.6 s and most have broad HWHM, with a median HWHM exceeding 0.35 μHz. Both our median $\ell = 1$ splitting of 13.5 μHz and median $\ell = 2$ splitting of 21.3 μHz suggest a roughly 11.2 hr rotation period, confirming that our mode identifications are internally self-consistent.

KIC 11911480 (KIS J1920+5017): This hot DAV (also cataloged as KIC 100003912) was thoroughly discussed in Greiss et al. (2014), who present an analysis of data from both Q12 and Q16, allowing for the identification of four of the five independent modes present. Here we only analyze data from Q16 but arrive at the same mode identifications.

EPIC 60017836 (GD 1212): We detailed our initial pulsation period list of GD 1212 in Hermes et al. (2014), which was the first published result using data from the two-wheel-controlled *K2* mission. After an extensive analysis using only the final nine days of the *K2* engineering data, we identified five of the modes present in the star, after concluding that the star rotates with a period of roughly 6.9 hr. At the top of Figure 13, we show the only identified $\ell = 1$ mode, f_3, which has a splitting of 21.3 μHz and is embedded within the $\ell = 2$ mode f_5. Additionally, we find two consecutive quadrupole modes
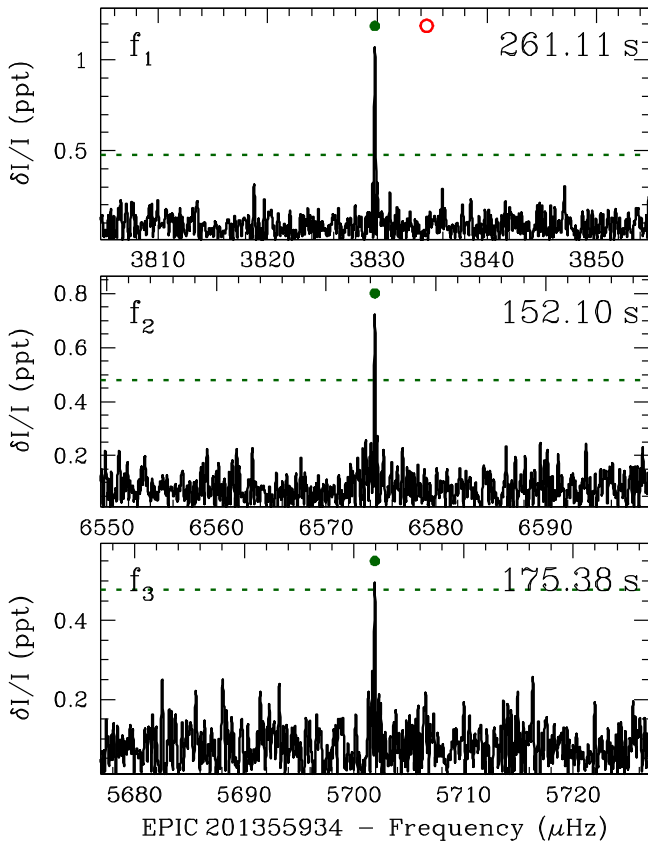
Figure 14. We show the three unidentified singlets in EPIC 201355934 (SDSS J1136−0136). We also mark with a red open circle the location of the only detected periodicity from ground-based discovery of pulsations in SDSS J1136 −0136 at 260.79 s (Castanheira et al. 2010).
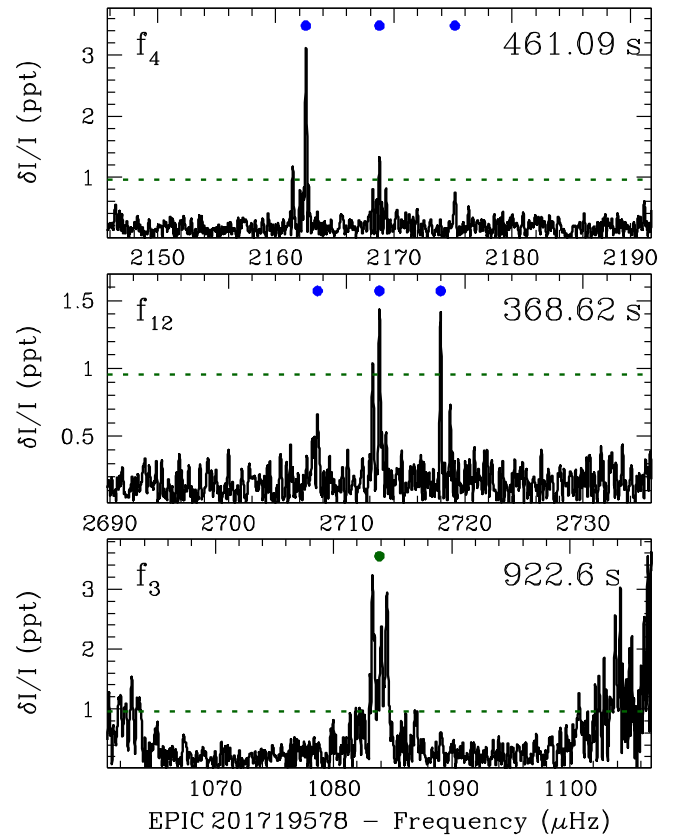

Figure 15. In the top panel, we show two identified dipole modes in EPIC 201719578 (SDSS J1122+0358); the median $\ell = 1$ splitting of 5.5 μHz reveals a 26.8 hr rotation period. The bottom panel shows a longer-period mode with a broader line width that we cannot definitively identify.

embedded within one another: f_2 and f_4; the median $\ell = 2$ splitting is 33.7 μHz. There are additional modes, including many nonlinear combination frequencies, presented in Hermes et al. (2014), from the full 11.5 days of engineering data on GD 1212, which were not significant from only this nine-day data set. We note that *K2* has revisited GD 1212 for more than 75 days during Campaign 12.

EPIC 201355934 (SDSS J1136−0136): We observe just three significant peaks in this DAV, all shown in Figure 14. None of the peaks appear to be components of the same k, ℓ multiplet, which means we cannot estimate the rotation period of this white dwarf; this is possible if the star is seen roughly pole-on, such that we only observe the $m = 0$ components. This DAV was known to pulsate before the launch of *Kepler*, but the only photometry is a discovery run yielding just one period at 260.79 s (Castanheira et al. 2010, shown by the open circle in Figure 14), nearest to f_1 in our *K2* observations.

EPIC 201719578 (SDSS J1122+0358): The periods in this cool DAV range from 367.9 to 1095.4 s, but only the three shortest-period modes are stable enough to be cleanly identified. We show in Figure 15 two of the $\ell = 1$ modes, which have a median splitting of 5.5 μHz, revealing this white dwarf's 26.8 hr rotation period. The bottom panel of Figure 15 shows the broader line width of a longer-period mode in the same star. It is unlikely that all 23 of the modes listed in Table 5 are independent modes. With an $\ell = 1$ splitting of 5.5 μHz, we would expect $\ell = 2$ splittings of roughly 8.6 μHz;

therefore, for example, f_3 and f_1 could be the $m = -2$ and $m = +1$ components, respectively, of the same $\ell = 2$ mode. There are therefore likely between 14 and 18 independent modes in this DAV, depending on how many of the unidentified modes are components of the same multiplet. Previous ground-based photometry from the discovery of pulsations showed two significant periodicities, at 859.0 and 996.1 s (Mukadam et al. 2004). We only see evidence for the mode f_2 at 861.4 ± 4.0 s in this *K2* data set (Table 5).

EPIC 201730811 (SDSS J1136+0409): The pulsations and light curve modeling of this DAV, which is the only pulsating white dwarf known in a post-common-envelope binary, were detailed in Hermes et al. (2015a). We excluded this DAV from Figure 8 since this white dwarf almost certainly interacted with its close dM companion, which currently orbits the DAV every 6.9 hr. We updated Table 5 to reflect our reanalysis of the pulsations: It appears that the two lowest-amplitude, longest-period oscillations are not independent modes but are likely difference frequencies (combination frequencies arising from nonlinear distortions in the atmosphere of the star). Specifically, it appears that the periodicity we called "f_6" in Hermes et al. (2015a) at 474.45 s is within the 1σ uncertainties of the difference frequency $f_5 - f_{4a}$. Additionally, what we called "f_7" at 395.91 s is within the 1σ uncertainties of the difference frequency $f_{3b} - f_{1c}$. Omitting both modes does not substantially alter the asteroseismic analysis (A. Bischoff-Kim 2016, private communication).
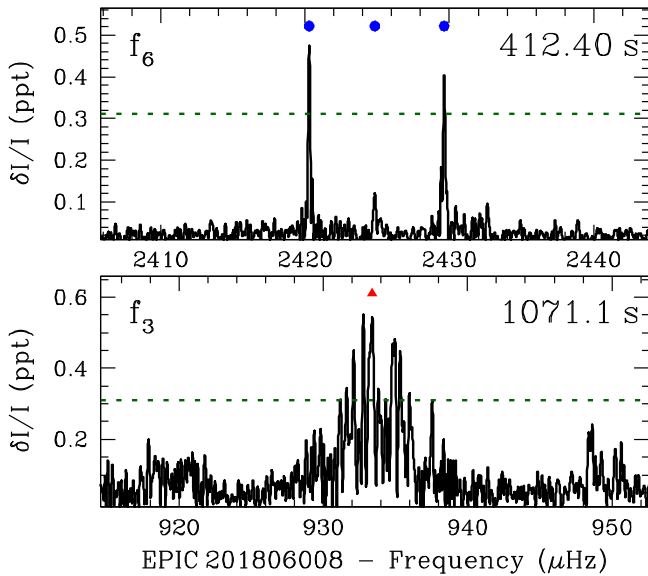
Figure 16. The top panel illuminates one of the identified dipole modes of EPIC 201806008 (PG 1149+057), which reveals the median $\ell = 1$ splitting of 4.7 μHz. This is the brightest outbursting DAV (Hermes et al. 2015b) and has many modes with very broad bands of power; the Fourier transforms shown here include all *K2* data collected, including data taken during outbursts. The bottom panel details a longer-period mode with a much broader line width.
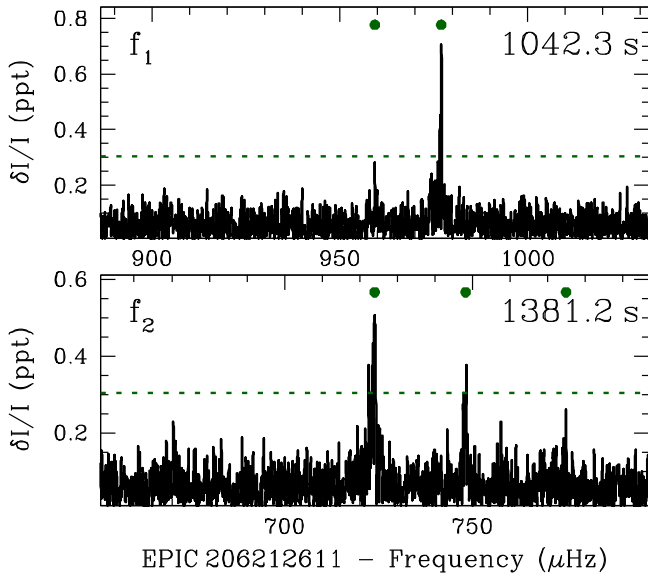

Figure 17. The two highest-amplitude sets of modes in EPIC 206212611 (SDSS J2220−0933) do not definitively reveal their identity. The two peaks in the top panel, which we refer to as f_1, suggest a possible $\ell = 1$ splitting 17.7 μHz, and the three peaks we refer to as f_2 have a roughly 26 μHz splitting, which would both correspond to a rotation period of roughly 8.3 hr. However, exclude this cool DAV from Section 7 and Figure 8, since we have not definitively identified the pulsations present.

EPIC 201802933 (SDSS J1151+0525): We showed the Fourier transforms of the five identified modes of this hot DAV, all of which are $\ell = 1$ modes, in Figure 1 in Section 3. Their median splitting is 4.7 μHz, which corresponds to a roughly 31.3 hr rotation period. It is possible that the mode f_6 at 123.18 s could suffer from the Nyquist ambiguity and instead be centered at 112.61 s; in all cases here, we selected the Nyquist alias with the highest amplitude, but this is not a guarantee they are the true signals in the star (Murphy 2015). Unfortunately, the *K2* observations only cover a small portion of the *Kepler* spacecraft
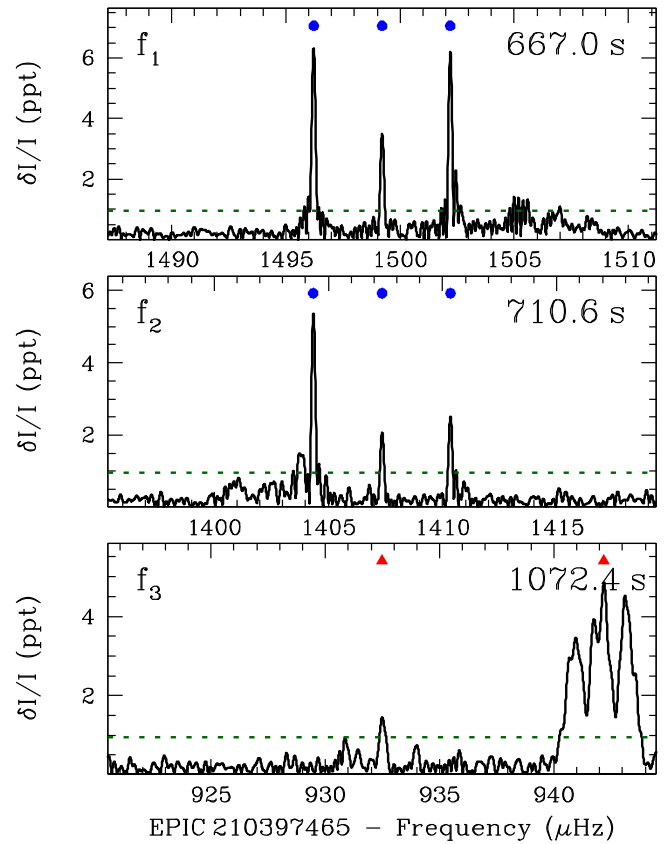
Figure 18. The top two panels show two $\ell = 1$ modes in EPIC 210397465 (SDSS J0358+1324), which share the median splitting of 3.0 μHz, suggesting a rotation period of roughly 49.1 hr. The bottom panel shows the likely $m = 0$ and $m = +2$ components of an $\ell = 2$ mode at a much longer period, corroborating the rotation rate; the $m = +2$ component is significantly broadened, with an HWHM = 0.963 μHz. Interestingly, both f_1 and f_2 show broad peaks outside the expected distribution for the $\ell = 1$ modes.

orbital motion, so we cannot search for incorrect Nyquist alias multiplet splittings at the orbital frequency of the spacecraft (Murphy et al. 2013). The Nyquist ambiguity for f_6 could be settled with follow-up, ground-based photometry, but for now we presume that the peaks centered around 123.18 s are the correct aliases.

EPIC 201806008 (PG 1149+057): We published an analysis of how outbursts affect the pulsations in this cool DAV in Hermes et al. (2015b), but did not thoroughly discuss the pulsations present in that letter. The Fourier transform we analyze here includes all *K2* data, including that taken in outburst. The shortest-period mode is most stable and reveals an apparent $\ell = 1$ splitting of 4.7 μHz (top panel of Figure 16), suggesting an overall rotation of 32.6 hr and commensurate $\ell = 2$ splittings of roughly 7.4 μHz. From this overall expectation, we tentatively identify 6 of the 14 independent modes present, most of which are highly broadened, an example of which is shown at the bottom panel of Figure 16. Excluding f_6 centered at 412.40 s, all other periods in this cool DAV range from 833.7 to 1392.1 s.

EPIC 206212611 (SDSS J2220−0933): We observe just six significant peaks in this DAV, ranging from 1023.4 to 1381.2 s, and we show five of these six peaks in Figure 17. It is difficult to identify the pulsations with so few modes, but it is possible that f_1 has a ∼17.7 μHz splitting and f_2 has a ∼26 μHz splitting, both of which correspond to a rotation period of roughly 8.3 hr if f_1 is an $\ell = 1$ mode and f_2 is an $\ell = 2$ mode. However, we did not
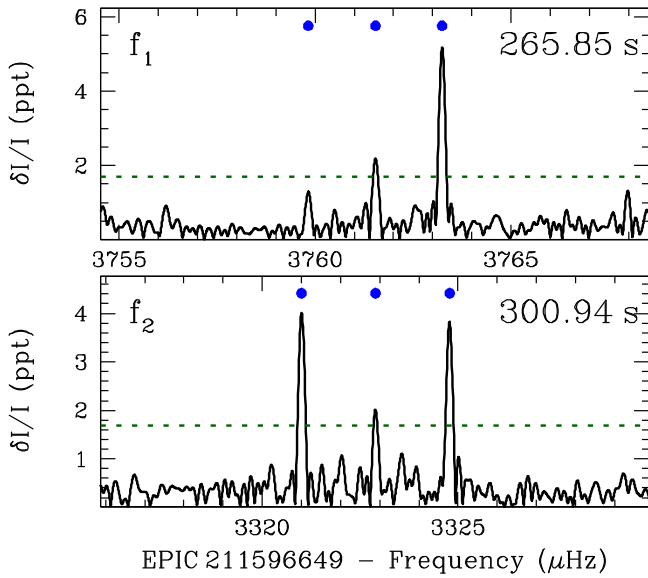
Figure 19. We show two modes in EPIC 211596649 (SDSS J0832+1429) that share the median $\ell = 1$ splitting of 1.8 μHz, corresponding to a relatively long rotation period of roughly 3.4 days.
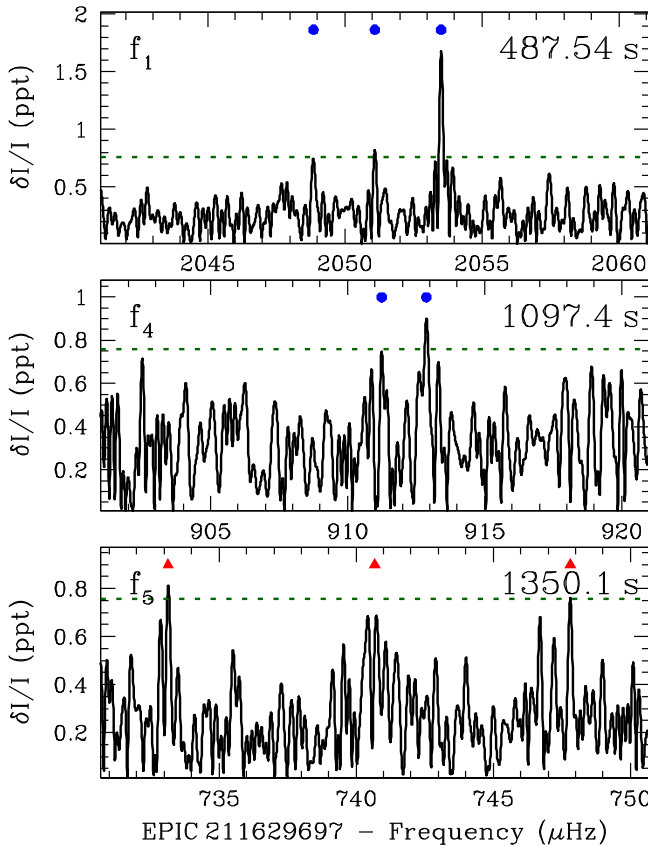

Figure 20. In the top panel, we show two dipole modes in EPIC 211629697 (SDSS J0840+1457), f_1 and f_4, which share the median $\ell = 1$ splitting of 2.3 μHz. The bottom panel shows what we identify as the $m = -2, 0, 2$ components of an $\ell = 2$ mode; the median $\ell = 2$ splittings of 3.6 μHz corroborate the roughly 64.0 hr rotation period in this outbursting DAV.

include this rotation period in our analysis in Section 7 because we lack certainty on the mode identification.

EPIC 210397465 (SDSS J0358+1324): We detect at least 10 nonlinear combination frequencies of this DAV, most of which
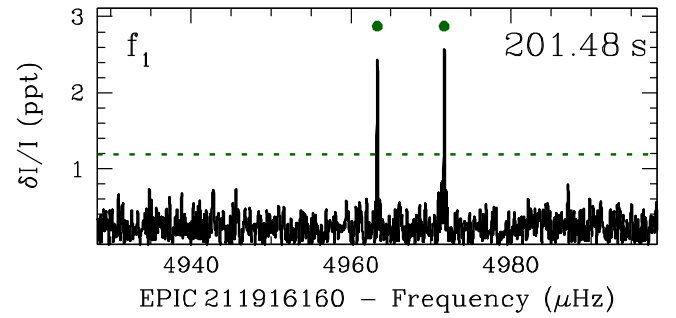
Figure 21. There are only two significant peaks in the Fourier transform of EPIC 211916160 (SDSS J0856+1858), separated by roughly 8.4 μHz, and so are likely components of the same independent mode in the star. However, we lack sufficient information to identify this mode at 201.48 s.
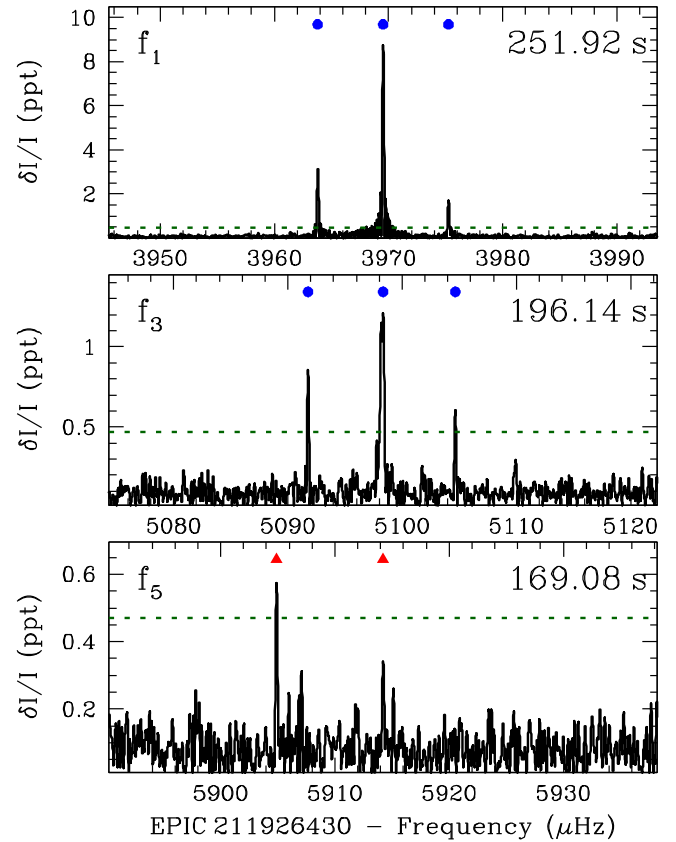
Figure 22. We show two modes in EPIC 211926430 (SDSS J0900+1907) in the top two panels which share the median $\ell = 1$ splitting of 5.8 μHz, corresponding to a rotation period of 25.4 hr. In the bottom panel, we show the likely $m = -1, 0$ components of an $\ell = 2$ mode in the star; the median $\ell = 2$ splitting of 9.1 μHz corroborates the 25.4 hr rotation.

involve either f_1 or f_2, which we identify as $\ell = 1$ modes and display in the top panels of Figure 18. The median $\ell = 1$ splitting of 3.0 μHz suggests a rotation period of 49.1 hr. We also observe three other multiplets that appear to have a median splitting of 4.7 μHz, exactly what we would expect for $\ell = 2$ splittings for a 49.1 hr rotation period; one such multiplet, f_3, is shown in the bottom panel of Figure 18. We are therefore able to identify 6 of the 11 independent modes present. The highest-amplitude modes at 667.0 s and 710.6 s have relatively narrow line widths, with HWHM <0.06 μHz, commensurate with the spectral window of the observations. However, both f_1 and f_2 show significant, broad, unidentified power; for f_1, this power is
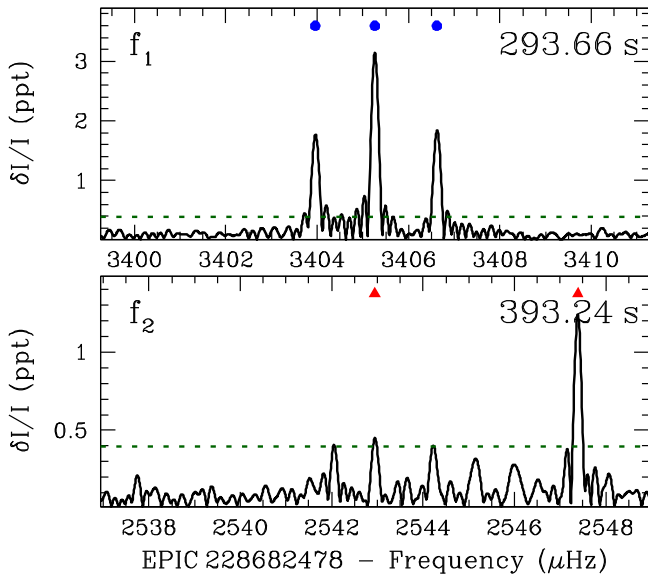
Figure 23. We show two modes in EPIC 228682478 (SDSS J0840+1320), both of which suggest an overall rotation period of roughly 113.3 hr: the $\ell = 1$ mode f_1 and the the $\ell = 2$ mode f_2. We only mark what appear to be the $m = 0, +2$ components of f_2, but there are other nearly significant signals around this mode that we do not identify.

Figure 24. We show two modes in EPIC 229227292 (ATLAS J1342−0735), including the $\ell = 1$ mode f_{13}, which shares the median $\ell = 1$ splitting of $5.0 \, \mu$Hz. Most other longer-period modes in this outbursting DAV have considerably broadened line widths, making mode identification more difficult.

Figure 25. We show two modes in EPIC 229228364 (SSS J1918−2621), which are broadened and have low amplitude. We see two bands of power in f_2 separated by roughly 6.3 μHz, but do not have enough additional information to establish mode identification for the three independent modes present in this outbursting DAV.

at a higher frequency than the $m = +1$ component, and in f_2 this power is at a lower frequency than the $m = -1$ component (Figure 18). As with KIC 7594781, further investigation of the frequency and amplitude stability of this DAV is warranted. We used the C/O-core models of Fontaine et al. (2001) to determine the mass of SDSS J0358+1324, but this DAV is very near the boundary for He-core white dwarfs.

EPIC 211596649 (SDSS J0832+1429): We observe just three independent modes in this DAV, two of which we identify as $\ell = 1$ modes and display in Figure 19. The median splitting of these peaks is 1.8 μHz, corresponding to a rotation period of 81.8 hr. It is possible that these three peaks are the $m = -2, 0, +2$ components of the $\ell = 2$ modes (which would arise if the white dwarf rotates at roughly 5.3 days). However, we prefer their identification as $\ell = 1$ modes given the increased geometric cancellation of $\ell = 2$ modes.

EPIC 211629697 (SDSS J0840+1457): We improved the extraction of this cool DAV from the discovery data described in Bell et al. (2016), who analyzed the outburst behavior, and present the analysis of the pulsations here. The shortest-period mode centered at 487.54 s informs our analysis of the patterns present in the modes, and we were able to identify seven of the eight independent modes observed in the star. The two top panels of Figure 20 reveal the highest-amplitude $\ell = 1$ modes, which have a median splitting of 2.3 μHz; this corresponds to a rotation period of 64.0 hr. We would expect $\ell = 2$ splittings of roughly 3.6 μHz from a 64 hr rotation period, which is exactly the splitting observed for the three peaks in f_5 shown in the bottom panel of Figure 20. Aside from the shorter-period f_1 centered at 487.54 s, the other significant modes in this cool DAV range from 1095.5 to 1364.0 s.

EPIC 211914185 (SDSS J0837+1856): We explored the pulsations of this massive DAV, including breaking the Nyquist ambiguity with follow-up, ground-based data, in Hermes et al. (2017c). Of the white dwarfs with rotation rates measured using
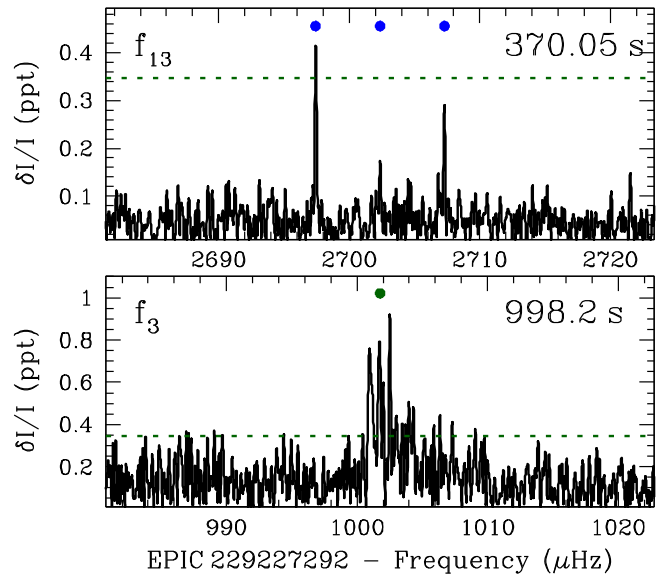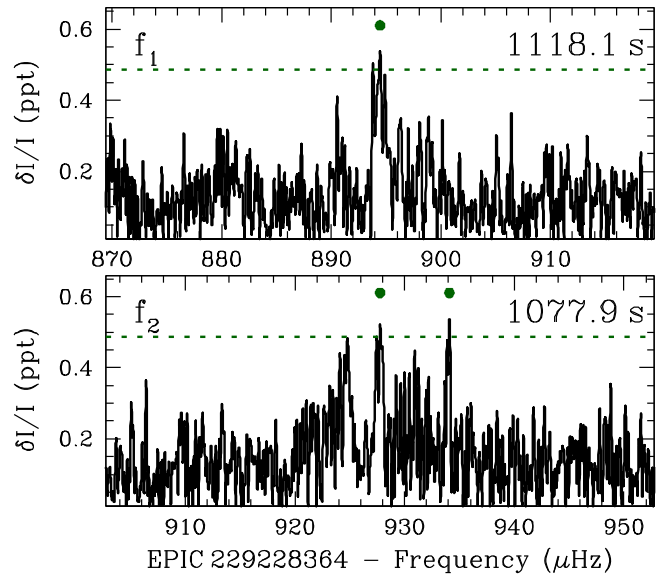
asteroseismology, it remains the most massive and fastest rotating, likely the descendant of a roughly $4.0 \, M_\odot$ ZAMS progenitor.

EPIC 211916160 (SDSS J0856+1858): We have the fewest asteroseismic constraints on this DAV, since we only detect one independent mode, which we show in Figure 21. The two significant peaks we detect are separated by roughly 8.4 μHz, but we have no other constraints, and therefore cannot identify the spherical degree of this mode and do not include it in our rotation analysis in Section 7. The simplest explanation is that these are either the $m = 0, +1$ or $m = -1, +1$ components of an $\ell = 1$ mode, which would correspond to a rotation period of either
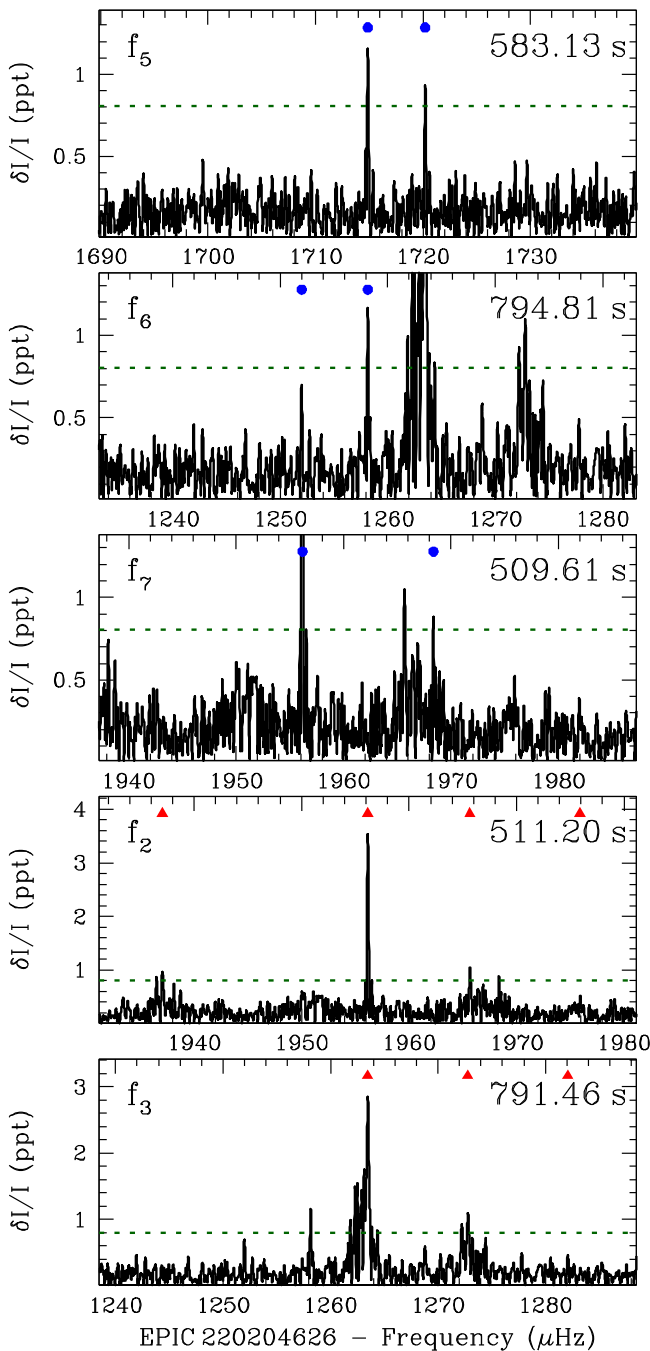
Figure 26. We show five modes in EPIC 220204626 (SDSS J0111+0009), some of which are closely overlapping, so we only mark the components of the respective multiplets with blue dots for the $\ell = 1$ modes and red triangles for the $\ell = 2$ modes. The splittings for all identified modes are consistent with an overall rotation period of roughly 24.3 hr.

Figure 27. The hot DAV EPIC 220258806 (SDSS J0106+0145) provides an exceptional case of mode identification via rotational splittings. We plot the two $\ell = 1$ modes, which share a median splitting of 4.9 μHz, as well as the two highest-amplitude $\ell = 2$ modes (red triangles), which share a median splitting of 7.7 μHz. Both sets of splittings corroborate an overall rotation period of 30.0 hr.

17.5 hr or 8.8 hr, respectively. However, for now, we leave f_1 unidentified and do not include this DAV in our rotation analysis.

EPIC 211926430 (SDSS J0900+1907): We are able to identify five of the six independent modes in this DAV. In the top two panels of Figure 22, we show the highest-amplitude $\ell = 1$ modes, which share the median splitting of 5.8 μHz, corresponding to a rotation period of 25.4 hr. We also observe two $\ell = 2$ modes with a median splitting of 9.1 μHz, fully consistent with the rotation period and confirming our mode identification. It is possible that the mode we observe centered

at 119.51 s is an incorrect Nyquist alias; the super-Nyquist alias of f_6 would instead be centered at roughly 115.96 s, which could be ruled out or confirmed with follow-up photometry. With a spectroscopically determined temperature of 11,420 K, this is the coolest DAV in our sample with a WMP shorter than 400 s; the periods we detect range from 119.51 to 299.58 s, with a WMP of 244.2 s. However, it does not appear to be a significant outlier in Figure 6.

EPIC 228682478 (SDSS J0840+1320): We identified two of the three independent modes in this DAV, which we display in Figure 23. Both of the splittings observed in the dipole mode f_1 (1.3 μHz) and the quadrupole mode f_2 (2.2 μHz) corroborate an overall rotation period of roughly 113.3 hr (4.5 days), the longest rotation period measured for any pulsating white dwarf. There are several other nearly significant signals around f_2 at 2544.231 $\pm$ 0.014 μH
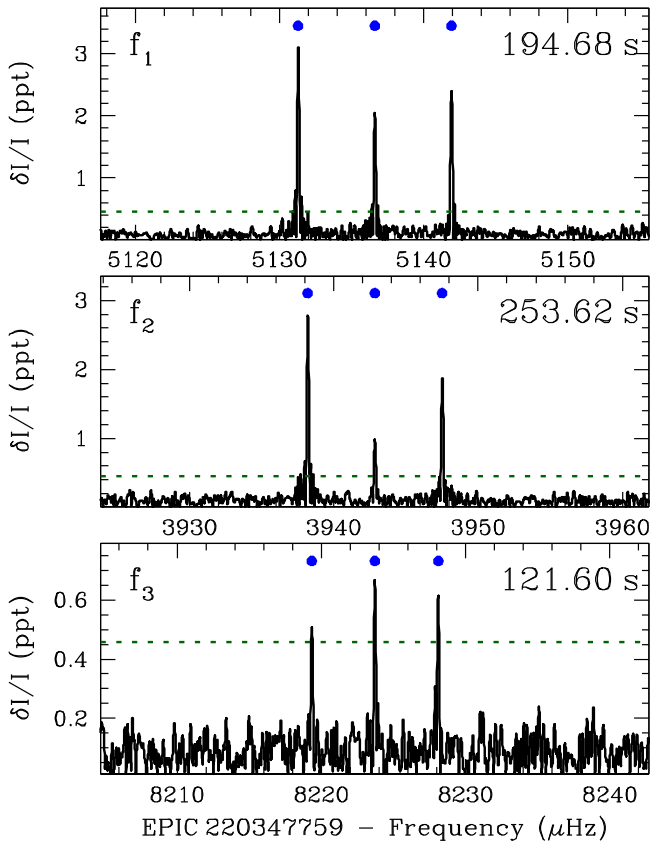
Figure 28. We show three modes in EPIC 220347759 (SDSS J0051+0339), all of which share roughly the median $\ell = 1$ splitting of 4.65 μHz.
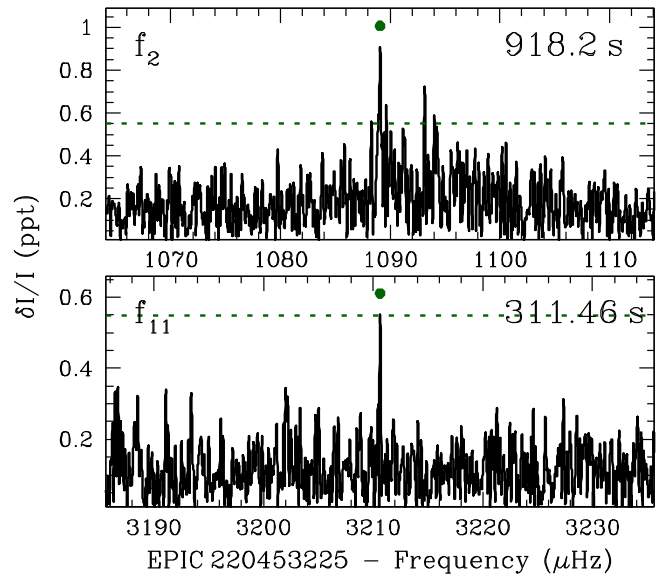

Figure 29. We show two modes in EPIC 220453225 (SDSS J0045+0544), neither of which we have been able to identify. This is the sixth outbursting DAV detected by the *Kepler* spacecraft (Bell et al. 2017).
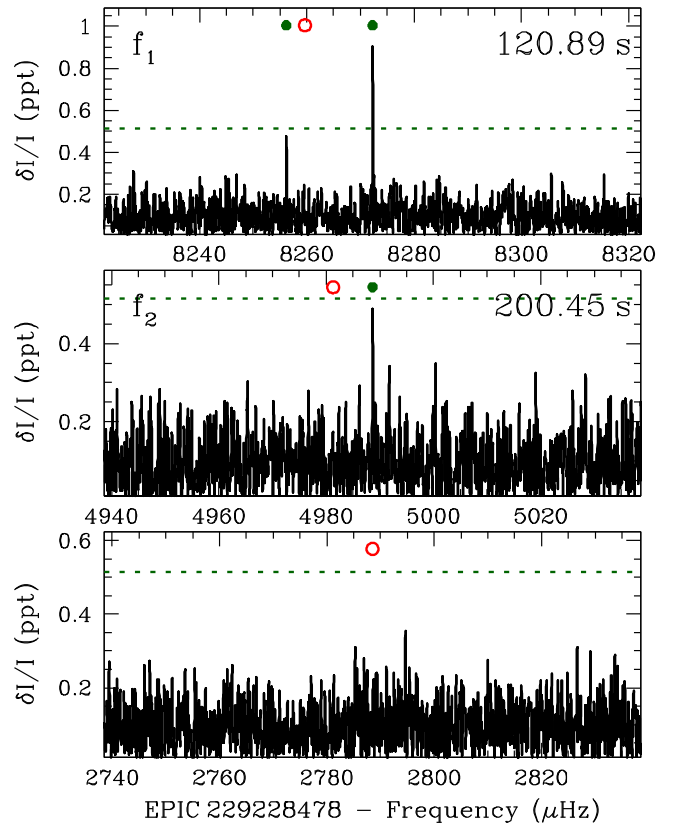

Figure 30. We show three frequency regions in the amplitude spectrum of EPIC 229228478 (SDSS J0122+0030). The open red circles denote the three periodicities detected from discovery photometry published by Castanheira et al. (2010); we discovered modes corresponding to the two highest-amplitude peaks from that work, but do not corroborate their mode at 358.6 s. We have not identified any of the modes present in this hot DAV.

(0.39 ± 0.07 ppt), 2542.053 ± 0.014 μHz (0.39 ± 0.07 ppt), 2545.152 ± 0.016 μHz (0.36 ± 0.07 ppt), and 2546.033 ± 0.019 μHz (0.30 ± 0.07 ppt). However, it is not clear if these represent an unfortunate confluence of noise (since none are formally significant), or if they represent multiplets from another independent mode around f_2, or if they are caused by some other means (such as the mysterious side peaks seen in f_1 and f_2 of EPIC 210397465).

EPIC 229227292 (ATLAS J1342−0735): We show two modes in this outbursting DAV in Figure 24; the outburst characteristics were described in Bell et al. (2016). We only identify 3 of the 18 independent modes in this rich pulsator, guided by the two short-period dipole modes at 370.05 s and 288.91 s, which share the median $\ell = 1$ splitting of 5.0 μHz. Aside from those two short-period modes, the additional pulsations range from 514.1 to 1323.6 s, many with broad bands of power, such as f_3 shown in Figure 24.

EPIC 229228364 (SSS J1918−2621): We detect at least six outbursts in this cool DAV, including a very long recurrence time between outbursts of at least 9.5 days (characterization of those outbursts will be presented in a forthcoming publication, as previewed in Bell et al. 2017). This DAV has the fewest pulsation modes of any outbursting DAV, with just three significant independent modes from 1070.6 to 1204.8 s (at $K_p = 17.9$ mag; this is not simply caused by low S/N). Only one of these three modes appears to be a multiplet, as seen in f_2 in the bottom panel of Figure 25; these modes are separated by 6.3 μHz. However, with just one incomplete multiplet, we cannot use it to inform our mode identification or rotation analysis.

EPIC 220204626 (SDSS J0111+0009): This DAV has a line-of-sight M2 companion, but from the 37 SDSS subspectra, we see no evidence of radial-velocity variability, so this is most
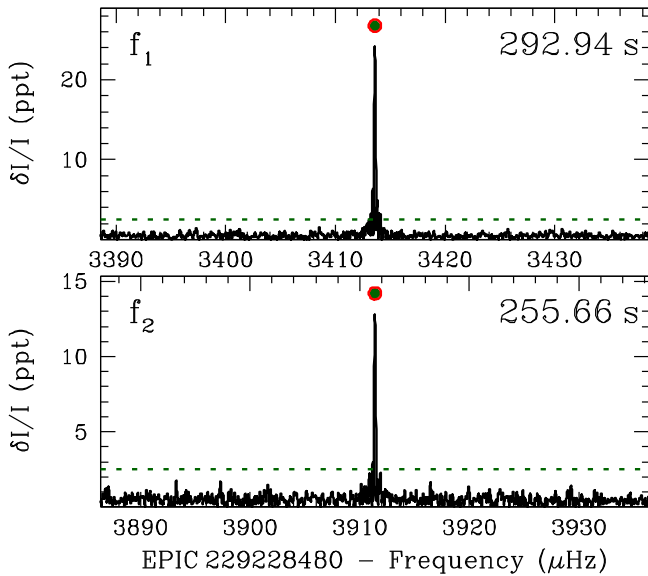
Figure 31. The hot DAV EPIC 229228480 (SDSS J0111+0018) shows just two independent modes, which appear as singlets. The periods determined from *K2* match exactly the periods determined from ground-based discovery (Mukadam et al. 2004) and follow-up (Hermes et al. 2013) photometry.

likely a wide binary (Rebassa-Mansergas et al. 2016); this is corroborated by the lack of any low-frequency variability in the *K2* data. The 2.8 hr discovery light curve obtained on 2010 December 8 (Pyrzas et al. 2015) found pulsations at periods of 631.6 s (28 ppt in *g'*), 583.2 s (16.3 ppt), 510.2 s (18.9 ppt), and 366.5 s (9.1 ppt). We see the three highest amplitudes of these periods in our *K2* data as f_4, f_5, and f_2, respectively. Our extended light curve allows us to identify five of the seven independent pulsations present, which we show in Figure 26. The periods in this DAV range from 506.09 to 798.73 s for a WMP of 642.7 s. The median $\ell = 1$ splitting of 6.1 μHz and median $\ell = 2$ splitting of 9.5 μHz are both consistent with a 24.3 hr rotation period. Many of the $\ell = 1$ and $\ell = 2$ modes are close together, and it appears that the $m = -1$ component of the dipole mode f_7 is very nearly overlapping in frequency with the $m = 0$ component of the quadrupole mode f_2, shown one after the other in Figure 26. Notably, the two $\ell = 2$ modes have much higher amplitudes than the three identified $\ell = 1$ modes, which is the opposite of what we would expect from geometric cancellation.

EPIC 220258806 (SDSS J0106+0145): This hot DAV yields a textbook case of mode identification via rotational splittings, as shown in Figure 27. We are able to identify 5 of the 11 independent periods present in the star. The two dipole modes have a median splitting of 4.9 μHz, and the three quadrupole modes have a median splitting of 7.7 μHz, which both independently reveal the rotation period of 30.0 hr. However, the two highest-amplitude modes appear as singlets and are not identified. There are two sets of signals very near the Nyquist frequency: the three peaks of f_5 have much higher amplitudes at the super-Nyquist position, so we use that Nyquist alias as the correct one in the star, whereas f_{11} appears highest below the Nyquist frequency. Using three nights of time-series photometry from SOAR, we confirm our selection of these aliases: we confirm that f_5 is super-Nyquist with periods centered at

116.49 s and that f_{11} is just below the Nyquist frequency, with a period of 119.88 s.

EPIC 220347759 (SDSS J0051+0339): We show the three highest-amplitude modes in Figure 28, all of which we identify as dipole modes with a median $\ell = 1$ splitting of 4.65 μHz. There is some crowding in the field, with a brighter ($\Delta K_p < 1.1$ mag) star less than 13″ from the target.

EPIC 220453225 (SDSS J0045+0544): We detected at least 15 outbursts in this cool DAV, which we will characterize in a forthcoming publication. We show in Figure 29 two different pulsations in the star: f_2 is representative of the longer-period pulsations present from 670.9 to 1391.5 s, and f_{11} at 311.46 s is a short-period mode also observed. We have not been able to solve any of the mode identifications for the 16 pulsations detected.

EPIC 229228478 (SDSS J0122+0030): A short run from discovery ground-based photometry published by Castanheira et al. (2010) revealed three periodicities in this DAV, at 121.1 s (1.5 ppt), 200.8 s (1.3 ppt), and 358.6 s (right at the significance threshold of 1.2 ppt). We detected two of these three ground-based modes, as shown in Figure 30, and show that the mode near 121.1 s is likely a multiplet split by roughly 16.1 μHz. However, with just two multiplet components, we cannot identify any modes. If we assume that f_1 is an $\ell = 1$ mode split by either 16.1 μHz or 8.0 μHz, that would correspond to an overall rotation rate of either 9.1 hr or 18.4 hr, respectively. However, since we lack firm mode identifications, we do not include this DAV in our rotation analysis.

EPIC 229228480 (SDSS J0111+0018): This hot DAV has been monitored with ground-based photometry for more than a decade, and its pulsations reveal a rate of period change inconsistent with secular cooling (Hermes et al. 2013). As with the long ground-based data sets, with *K2* we see only two independent modes that appear as singlets, shown in Figure 31, as well as nonlinear combination frequencies of those two modes. It is possible that this DAV is seen pole-on, such that only the $m = 0$ components are visible; without multiplets, we cannot constrain mode identification.

9. Discussion and Conclusions

We present here the first bulk reduction and analysis of data collected on 27 pulsating DA white dwarfs observed by the *Kepler* space telescope up to *K2* Campaign 8. This long-duration, high duty cycle photometry provides a way to securely resolve and identify hundreds of modes in DAVs without aliasing problems. The total baseline of data collected by *Kepler* and *K2* on DAVs already exceeds the sum total of ground-based optical photometry acquired since their identification as a class by McGraw (1979).

The data sets analyzed here represent an extensive series of observations. The centerpiece is more than 2.75 million minute-cadence exposures collected during both the original *Kepler* mission as well as *K2*, yielding more than 45,000 hr (1875 days) of space-based photometry of 27 pulsating white dwarfs. We also obtained more than 140 new spectra collected over 15 separate nights with the 4.1 m SOAR telescope in order to characterize the atmospheric parameters of the entire sample, yielding external estimates of the white dwarf effective temperature and surface gravity, and thus overall white dwarf mass.

Our target selection is relatively unbiased; given the sparseness of white dwarfs observed by *K2* so far, we propose many candidates for short-cadence photometry, most based on either serendipitous SDSS spectra or appropriate $(u-g, g-r)$ colors. We therefore find pulsating white dwarfs throughout all regions of the DAV instability strip, spanning the stable, short-period hot DAVs at the hot edge of the strip all the way down to the coolest DAVs with the longest-period pulsations.

Our efforts in this paper have narrowly focused on the observational insights revealed from *Kepler* and now *K2*, leaving asteroseismic analysis of these stars to future publications. However, we noticed some exceptional patterns just from direct analysis of these unique observations that are free of diurnal aliasing that complicate ground-based observations.

We discovered a significant dichotomy of mode line widths, often within the same star, which appear almost completely related to the period of pulsation variability. Almost all pulsations with periods less than 800 s appear to show relatively narrow line widths; Lorentzian fits find that their HWHM is comparable to the spectral window. However, most modes exceeding 800 s show highly broadened line widths, many of which resemble stochastic oscillators like the Sun. The measured HWHM of Lorentzian fits to these long-period modes correspond to the *e*-folding timescale of order days to weeks, in line with expected growth (and damping) rates for high radial-order modes. We are exploring a consistent physical model to explain these broad line widths (M. H. Montgomery et al. 2017, in preparation).

We were also able to identify the spherical degree (ℓ) of more than 40% of the 201 independent modes present in these 27 DAVs, based on frequency patterns caused by rotational splittings. We are therefore able to measure the internal rotation (still confined to at least the outer 1% of the star) for 20 of the 27 DAVs observed so far with the *Kepler* spacecraft.

Although we have not performed any asteroseismic fits on our sample (and many of these DAVs show just a few independent modes), we are able to use our follow-up spectroscopic observations to constrain, for the first time in a systematic way, white dwarf rotation as a function of mass. We find that white dwarfs with masses between 0.51 and 0.74 $M_\odot$ (within 1σ of the field white dwarf mass distribution) have a mean rotation period of 35 hr and a standard deviation of 28 hr. Using cluster-calibrated initial-to-final mass relations, such white dwarfs evolved from 1.7 to 3.0 $M_\odot$ ZAMS progenitors. Therefore, we are putting narrowing boundary conditions on the endpoints of angular momentum evolution in the range of masses probed deeply by the *Kepler* spacecraft in earlier stages of stellar evolution. Given the slow rotation of apparently isolated white dwarfs, it thus appears from *Kepler* that most internal angular momentum is lost on the first-ascent giant branch. We hope that bulk white dwarf rotation rates as a function of mass can shed further light on the unknown angular momentum transport mechanism coupling red-giant cores to their envelopes, especially the timescale of the coupling required to match internal rotation at all late stages of stellar evolution (e.g., Tayar & Pinsonneault 2013; Cantiello et al. 2014).

Kepler photometry has shed insight into what appear to be at least five stages of DAV evolution, which we summarize in Figure 7. Pulsation amplitudes start relatively low at the blue edge of the DAV instability strip, grow as the star cools, and eventually reach very high amplitudes when the star reaches the middle of the instability strip. We generally confirm the observational trend that cooler DAVs have longer pulsation periods, predicted from the theory that as white dwarfs cool, their convection zones deepen and thus have a longer thermal adjustment timescale.

We also observe from *Kepler* and *K2* observations that nonlinear combination frequencies are most often visible for stars nearer the middle of the instability strip. We observe these nonlinear artifacts in only 8 of the 27 DAVs here. Six of the eight with nonlinear combination frequencies cluster in a relatively narrow region of the instability strip, with a WMP ranging from 248.4 to 358.1 s and spectroscopic temperatures ranging from 12,750 to 11,880 K. However, we do not observe nonlinear combination frequencies in any of the six outbursting DAVs so far. There are just two relatively cool DAVs showing combination frequencies: GD 1212 (11,280 K, WMP = 1019.1 s, with combinations detailed in Hermes et al. 2014) and EPIC 210397465 (11,520 K, WMP = 841.0 s). Although we are not as sensitive to the highest-frequency nonlinear combinations given that the Nyquist frequency falls at roughly 8496.18 μHz, we have shown from some of our DAVs that we can detect super-Nyquist signals. Thus, we have confidence in our assertion that it appears that, for most cases, the observed nonlinear combination frequencies are restricted to a relatively narrow range of the instability strip, seen most often for the highest-amplitude DAVs in the middle of the instability strip.

K2 will continue to observe new fields along the ecliptic until it runs out of fuel, which is projected to occur at some point between Campaigns 17–19. With continued proposal success, we expect to observe more than 150 additional candidate pulsating white dwarfs from Campaign 9 until the end of the mission, leaving a large legacy data set of white dwarf variability. We venture to maintain this and future DAV data sets online at http://k2wd.org, where we have collected the raw and reduced *Kepler* light curves as well as the raw and reduced spectroscopy for the community to directly explore and (re)analyze.

Facilities: Kepler, *K2*, SOAR, SDSS.

APPENDIX

Table 5
Pulsation Information from Linear Least-squares (LLS; Section 3) and Lorentzian (Lor.; Section 5) Fits for the First 27 DAVs Observed by *Kepler* and *K2*

KIC/EPIC	Mode	LLS Per. (s)	ΔPer. (s)	LLS Freq. (μhz)	ΔFreq. (μhz)	Amp. (ppt)	ΔAmp. (ppt)	Phase (rad.)	ΔPhase (rad.)	Lor. Per. (s)	ΔPer. (s)	HWHM (μhz)	Lor. Amp. (ppt^2)	Splitting (μhz)	ℓ	m
4357037	f_{1a}	317.42718	0.00022	3150.3288	0.0021	12.41	0.15	0.6177	0.0019	317.427	0.011	0.108	172.777	⋯	1	−1
4357037	f_{1b}	316.8081	0.0013	3156.485	0.013	1.98	0.15	0.299	0.012	316.808	0.011	0.105	5.051	6.156	1	0
4357037	f_{1c}	316.19259	0.00018	3162.6294	0.0018	14.39	0.15	0.3086	0.0017	316.193	0.011	0.108	231.339	6.145	1	1
4357037	f_{2a}	346.22018	0.00056	2888.3354	0.0047	5.66	0.15	0.3463	0.0043	346.220	0.013	0.108	35.069	⋯	1	−1
4357037	f_{2b}	345.3365	0.0030	2895.726	0.025	1.06	0.15	0.451	0.023	345.338	0.012	0.098	1.359	7.391	1	0

(This table is available in its entirety in machine-readable form.)

ORCID iDs

Steven D. Kawaler ⓘ https://orcid.org/0000-0002-6536-6367
P.-E. Tremblay ⓘ https://orcid.org/0000-0001-9873-0121
Keaton J. Bell ⓘ https://orcid.org/0000-0002-0656-032X
E. Dennihy ⓘ https://orcid.org/0000-0003-2852-268X
B. H. Dunlap ⓘ https://orcid.org/0000-0002-1086-8685
M. H. Montgomery ⓘ https://orcid.org/0000-0002-6748-1748
T. R. Marsh ⓘ https://orcid.org/0000-0002-2498-7589
S. Redfield ⓘ https://orcid.org/0000-0003-3786-3486

References

Aerts, C. 2015, AN, 336, 477
Althaus, L. G., Córsico, A. H., Isern, J., & García-Berro, E. 2010, A&ARv, 18, 471
Antoci, V., Handler, G., Campante, T. L., et al. 2011, Natur, 477, 570
Bell, K. J., Hermes, J. J., Bischoff-Kim, A., et al. 2015, ApJ, 809, 14
Bell, K. J., Hermes, J. J., Montgomery, M. H., et al. 2016, ApJ, 829, 82
Bell, K. J., Hermes, J. J., Montgomery, M. H., et al. 2017, in ASP Conf. Ser. 509, 20th European White Dwarf Workshop, ed. P.-E. Tremblay, B. Gaensicke, & T. Marsh (San Francisco, CA: ASP), 303
Bognár, Z., Paparó, M., Molnár, L., et al. 2016, MNRAS, 461, 4059
Bond, H. E., Kawaler, S. D., Ciardullo, R., et al. 1996, AJ, 112, 2699
Bradley, P. A. 2001, ApJ, 552, 326
Brassard, P., Fontaine, G., Wesemael, F., & Hansen, C. J. 1992, ApJS, 80, 369
Brickhill, A. J. 1991, MNRAS, 251, 673
Brickhill, A. J. 1992, MNRAS, 259, 519
Brown, T. M., Latham, D. W., Everett, M. E., & Esquerdo, G. A. 2011, AJ, 142, 112
Cantiello, M., Mankovich, C., Bildsten, L., Christensen-Dalsgaard, J., & Paxton, B. 2014, ApJ, 788, 93
Castanheira, B. G., Kepler, S. O., Kleinman, S. J., Nitta, A., & Fraga, L. 2010, MNRAS, 405, 2561
Castanheira, B. G., Kepler, S. O., Kleinman, S. J., Nitta, A., & Fraga, L. 2013, MNRAS, 430, 50
Chaplin, W. J., Houdek, G., Karoff, C., Elsworth, Y., & New, R. 2009, A&A, 500, L21
Chaplin, W. J., & Miglio, A. 2013, ARA&A, 51, 353
Charpinet, S., Fontaine, G., & Brassard, P. 2009, Natur, 461, 501
Clemens, J. C. 1993, BaltA, 2, 407
Clemens, J. C. 1994, PhD thesis, Texas Univ.
Clemens, J. C., Crain, J. A., & Anderson, R. 2004, Proc. SPIE, 5492, 331
Cummings, J. D., Kalirai, J. S., Tremblay, P.-E., & Ramirez-Ruiz, E. 2016, ApJ, 818, 84
Currie, M. J., Berry, D. S., Jenness, T., et al. 2014, in ASP Conf. Ser. 485, Astronomical Data Analysis Software and Systems XXIII, ed. N. Manset & P. Forshay (San Francisco, CA: ASP), 391
Davies, G. R., Handberg, R., Miglio, A., et al. 2014, MNRAS, 445, L94
Degroote, P., Aerts, C., Baglin, A., et al. 2010, Natur, 464, 259
Deheuvels, S., Ballot, J., Beck, P. G., et al. 2015, A&A, 580, A96
Dolez, N., Vauclair, G., Kleinman, S. J., et al. 2006, A&A, 446, 237
Everett, M. E., Howell, S. B., & Kinemuchi, K. 2012, PASP, 124, 316
Fontaine, G., & Brassard, P. 2008, PASP, 120, 1043
Fontaine, G., Brassard, P., & Bergeron, P. 2001, PASP, 113, 409
Fu, J.-N., Dolez, N., Vauclair, G., et al. 2013, MNRAS, 429, 1585
Fu, J.-N., Vauclair, G., Solheim, J.-E., et al. 2007, A&A, 467, 237
Gentile Fusillo, N. P., Gänsicke, B. T., & Greiss, S. 2015, MNRAS, 448, 2260
Gentile Fusillo, N. P., Raddi, R., Gänsicke, B. T., et al. 2017, MNRAS, 469, 621
Giammichele, N., Fontaine, G., Brassard, P., & Charpinet, S. 2016, ApJS, 223, 10
Gianninas, A., Bergeron, P., & Fontaine, G. 2006, AJ, 132, 831
Gianninas, A., Bergeron, P., & Ruiz, M. T. 2011, ApJ, 743, 138
Gilliland, R. L., Jenkins, J. M., Borucki, W. J., et al. 2010, ApJL, 713, L160
Goldreich, P., & Wu, Y. 1999, ApJ, 511, 904
Greiss, S., Gänsicke, B. T., Hermes, J. J., et al. 2014, MNRAS, 438, 3086
Greiss, S., Hermes, J. J., Gänsicke, B. T., et al. 2016, MNRAS, 457, 2855
Greiss, S., Steeghs, D., Gänsicke, B. T., et al. 2012, AJ, 144, 24
Hermes, J. J., Charpinet, S., Barclay, T., et al. 2014, ApJ, 789, 85
Hermes, J. J., Gänsicke, B. T., Bischoff-Kim, A., et al. 2015a, MNRAS, 451, 1701
Hermes, J. J., Gänsicke, B. T., Gentile Fusillo, N. P., et al. 2017a, MNRAS, 468, 1946
Hermes, J. J., Kawaler, S. D., Bischoff-Kim, A., et al. 2017b, ApJ, 835, 277
Hermes, J. J., Kawaler, S. D., Romero, A. D., et al. 2017c, ApJL, 841, L2
Hermes, J. J., Montgomery, M. H., Bell, K. J., et al. 2015b, ApJL, 810, L5
Hermes, J. J., Montgomery, M. H., Mullally, F., Winget, D. E., & Bischoff-Kim, A. 2013, ApJ, 766, 42
Hermes, J. J., Mullally, F., Østensen, R. H., et al. 2011, ApJL, 741, L16
Horne, K. 1986, PASP, 98, 609
Howell, S. B., Sobeck, C., Haas, M., et al. 2014, PASP, 126, 398
Kawaler, S. D. 2004, in IAU Symp. 215, Stellar Rotation, ed. A. Maeder & P. Eenens (San Francisco, CA: ASP), 561
Kawaler, S. D. 2015, in ASP Conf. Ser. 493, 19th European Workshop on White Dwarfs, ed. P. Dufour, P. Bergeron, & G. Fontaine (San Francisco, CA: ASP), 65
Kawaler, S. D., O'Brien, M. S., Clemens, J. C., et al. 1995, ApJ, 450, 350
Kepler, S. O., Giovannini, O., Wood, M. A., et al. 1995, ApJ, 447, 874
Kepler, S. O., Mukadam, A., Winget, D. E., et al. 2000, ApJ, 534, L185
Kleinman, S. J., Kepler, S. O., Koester, D., et al. 2013, ApJS, 204, 5
Kleinman, S. J., Nather, R. E., Winget, D. E., et al. 1998, ApJ, 495, 424
Koester, D., Dreizler, S., Weidemann, V., & Allard, N. F. 1998, A&A, 338, 612
Landolt, A. U. 1968, ApJ, 153, 151
Ledoux, P. 1951, ApJ, 114, 373
Lenz, P., & Breger, M. 2005, CoAst, 146, 53
Liebert, J., Bergeron, P., & Holberg, J. B. 2005, ApJS, 156, 47
Marques, J. P., Goupil, M. J., Lebreton, Y., et al. 2013, A&A, 549, A74
Marsh, T. R. 1989, PASP, 101, 1032
McGraw, J. T. 1979, ApJ, 229, 203
Montgomery, M. H. 2005, ApJ, 633, 1142
Mosser, B., Goupil, M. J., Belkacem, K., et al. 2012, A&A, 548, A10
Mukadam, A. S., Montgomery, M. H., Winget, D. E., Kepler, S. O., & Clemens, J. C. 2006, ApJ, 640, 956
Mukadam, A. S., Mullally, F., Nather, R. E., et al. 2004, ApJ, 607, 982
Murphy, S. J. 2015, MNRAS, 453, 2569
Murphy, S. J., Shibahashi, H., & Kurtz, D. W. 2013, MNRAS, 430, 2986
Nather, R. E., Winget, D. E., Clemens, J. C., Hansen, C. J., & Hine, B. P. 1990, ApJ, 361, 309
O'Brien, M. S., Vauclair, G., Kawaler, S. D., et al. 1998, ApJ, 495, 458
Østensen, R. H., Bloemen, S., Vučković, M., et al. 2011, ApJL, 736, L39
Østensen, R. H., Reed, M. D., Baran, A. S., & Telting, J. H. 2014, A&A, 564, L14
Østensen, R. H., Silvotti, R., Charpinet, S., et al. 2010, MNRAS, 409, 1470
Pech, D., & Vauclair, G. 2006, A&A, 453, 219
Pfeiffer, B., Vauclair, G., Dolez, N., et al. 1996, A&A, 314, 182
Pyrzas, S., Gänsicke, B. T., Hermes, J. J., et al. 2015, MNRAS, 447, 691
Rebassa-Mansergas, A., Ren, J. J., Parsons, S. G., et al. 2016, MNRAS, 458, 3808
Reed, M. D., Baran, A., Quint, A. C., et al. 2011, MNRAS, 414, 2885
Renedo, I., Althaus, L. G., Miller Bertolami, M. M., et al. 2010, ApJ, 717, 183
Robinson, E. L., Mailloux, T. M., Zhang, E., et al. 1995, ApJ, 438, 908
Romero, A. D., Córsico, A. H., Althaus, L. G., et al. 2012, MNRAS, 420, 1462
Rowell, N., & Hambly, N. C. 2011, MNRAS, 417, 93
Smith, J. C., Stumpe, M. C., Van Cleve, J. E., et al. 2012, PASP, 124, 1000
Still, M., & Barclay, T. 2012, PyKE: Reduction and analysis of Kepler Simple Aperture Photometry data, Astrophysics Source Code Library, ascl:1208.004
Stumpe, M. C., Smith, J. C., Van Cleve, J. E., et al. 2012, PASP, 124, 985
Su, J., Li, Y., Fu, J.-N., & Li, C. 2014, MNRAS, 437, 2566
Tayar, J., & Pinsonneault, M. H. 2013, ApJL, 775, L1
Toutain, T., & Appourchaux, T. 1994, A&A, 289, 649
Tremblay, P.-E., Bergeron, P., & Gianninas, A. 2011, ApJ, 730, 128
Tremblay, P.-E., Cummings, J., Kalirai, J. S., et al. 2016, MNRAS, 461, 2100
Tremblay, P.-E., Gianninas, A., Kilic, M., et al. 2015, ApJ, 809, 148
Tremblay, P.-E., Ludwig, H.-G., Steffen, M., & Freytag, B. 2013, A&A, 559, A104
Unno, W., Osaki, Y., Ando, H., Saio, H., & Shibahashi, H. 1989, Nonradial oscillations of stars
Van Grootel, V., Fontaine, G., Brassard, P., & Dupret, M.-A. 2013, ApJ, 762, 57
Vanderburg, A., & Johnson, J. A. 2014, PASP, 126, 948
Vauclair, G., Moskalik, P., Pfeiffer, B., et al. 2002, A&A, 381, 122
Voss, B., Koester, D., Østensen, R., et al. 2006, A&A, 450, 1061
Warner, B., & Robinson, E. L. 1972, NPhS, 239, 2
Winget, D. E., & Kepler, S. O. 2008, ARA&A, 46, 157
Winget, D. E., Nather, R. E., Clemens, J. C., et al. 1991, ApJ, 378, 326
Winget, D. E., Nather, R. E., Clemens, J. C., et al. 1994, ApJ, 430, 839
Wu, Y., & Goldreich, P. 1999, ApJ, 519, 783
Zong, W., Charpinet, S., Vauclair, G., Giammichele, N., & Van Grootel, V. 2016, A&A, 585, A22